The role of Dentin Sialophosphoprotein (DSPP) in craniofacial development

by

Carlos Alberto dos Santos Figueredo Junior

A thesis submitted in partial fulfillment of the requirements for the degree of

Master of Science

Medical Sciences - Oral Biology
University of Alberta

Abstract

Mineralized tissues of the body are composed of organic and inorganic matter. The organic matter forms the framework necessary for the inorganic matter to mineralize. Dentin sialophosphoprotein (DSPP) is known to be extremely important in the formation of dentin. In DSPP absence, a severely hypomineralized dentin is formed, in two conditions known as dentinogenesis imperfecta (DGI) and dentin dysplasia (DD). DSPP has recently been found in several non-dental tissues, including the mandibular condylar cartilage (MCC) and craniofacial skeleton. However, there is limited literature on the role of DSPP in these tissues.

To explore the role of DSPP in the craniofacial complex, two mice strains, DSPP knockout (DSPP-/-) and wild type (C57BL/6J), were compared at 1, 3 and 6 months of age. Long bones, skulls, and hemi-mandibles were used for investigation. Morphological analysis was composed of radiographic images, micro-computed tomography reconstructions and dual-energy x-rays analyses. Histological analysis was composed of hematoxylin and eosin staining and immunohistochemistry. Cell culture was also conducted to investigate the potential effects of DSPP absence in osteoblasts from the calvaria.

Results from this investigation showed mineralization defects in the structures of alveolar bones, skulls, and MCC, with the most significant impact at 1 month of age. In addition, hematoxylin and eosin staining showed what differences in tissue histology were potentially related to large scale anatomical changes.

This study concluded that DSPP is an essential protein for the normal mineralization of craniofacial tissues. Furthermore, it was shown that DSPP absence caused defects in the mineralization of skulls, MCC, and alveolar bones at the early stages of development.

Table of Contents

List of Figures

Abbreviations

BMD: bone mineral density.

BP: base pairs.

BSP: bonesialoprotein.

CO2: carbon dioxide.

DD: dentin dysplasia.

DGI: dentinogenesis imperfecta.

DMEM: Dulbecco's modified eagle medium.

DMP1: dentin matrix protein 1.

DNA: deoxyribonucleic acid.

DPP: dentin phosphoprotein.

DSP: dentin sialoprotein.

DSPP: dentin sialophosphoprotein.

DXA: dual-energy x-ray absorptiometry.

ECM: extracellular matrix.

EDTA: ethylenediaminetetraacetic acid.

ETS: electrolyzed total solution.

H&E: hematoxylin and eosin.

HA: hydroxiapatitie.

IHC: immunohistochemistry.

KO: knockout.

MCC: mandibular condylar cartilage.

mg: milligrams.

micro-CT: micro-computed tomography.

MIM Mendelian Inheritance of Man.

ml: milliliters.

NCP: non-collagenous protein.

nm: nanometers.

◦ **C:** degrees Celcius.

OPN: osteopontin.

PBS: phosphate-buffered saline.

PCR: polymerase chain reaction.

PDL: periodontal ligament.

PFA: paraformaldehyde.

PTM: post-traslational modification.

RT: room temperature.

SIBLING: small integrin-binding ligand n-glycosylated.

TAE: Tris-acetate-EDTA.

TE: Tris-EDTA.

TMJ: temporomandibular joint.

ul: microliters.

UV: ultraviolet.

Chapter 1

Introduction

There are four types of mineralized tissues in our body: bone, cementum, dentin, and enamel. [1] These tissues are predominantly made of inorganic matter, primarily found in the form of hydroxyapatite (HA) crystals. Organic matter is also present, found in the form of collagen and non-collagenous proteins (NCPs). These proteins function to create the framework for the inorganic matter to mineralize. [2][3]

1.1 Bone

1.1.1 Composition

Bone is comprised of 60% inorganic matter, where the majority are made of HA crystals. Organic matter is found in 30%, with 90% of this material containing collagen, and 5-10% are NCPs. The remaining 10% of the bone composition is found as water. [4] The quantity, quality, and organization of each of these components define the quality of bone tissue. [5] Bone mineral density (BMD) is defined as the amount of bone (weight) divided by a selected region (area). [5] BMD is a standard measurement used to predict a bone's tendency to fracture and define the quality of bone. [5][6] Bone quality also takes the mineralization of bone into account, which translates as the organization and size of HA crystals. [4] The bone composition is illustrated in figure 1.1.

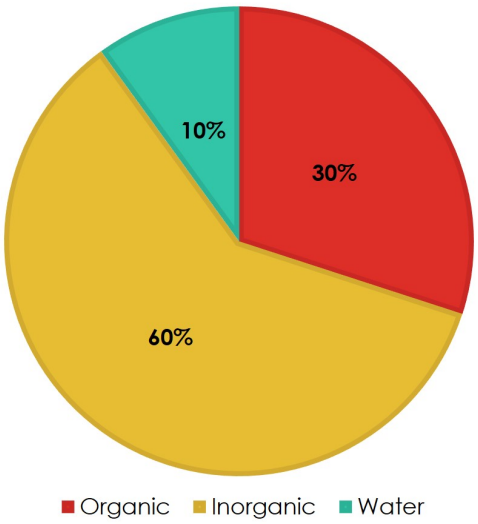

Figure 1.1: Bone composition.

1.1.2 Formation

Bone formation follows two different pathways. In intramembranous ossification, bone development occurs directly from mesenchymal connective tissue. Intramembranous ossification is responsible for the formation of most of the cranium. [7] On the other hand, in endochondral ossification, bone development occurs by replacing hyaline cartilage. Endochondral ossification is responsible for long bones and the base of the skull formation. [7]

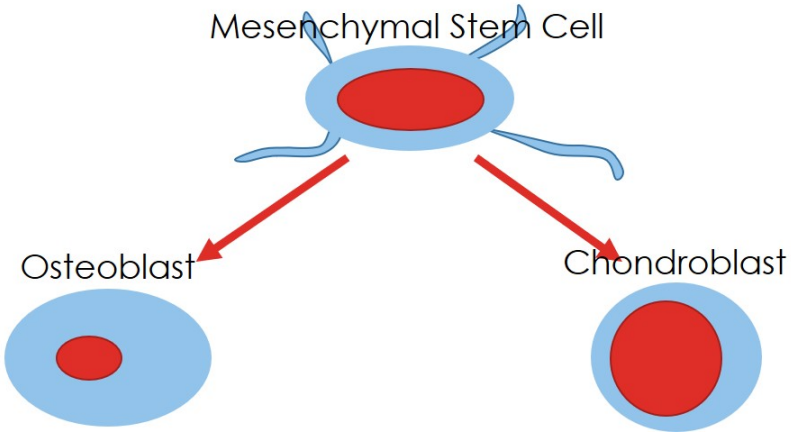

Figure 1.2: Mesenchymal Stem Cell differentiation. A mesenchymal stem cell has the potential to differentiate into an osteoblast (for intramembranous ossification) or chondroblast (for endochondral ossification).

1.1.3 Alveolar bone

The maxilla and mandible bones are divided into the basal body and the alveolar processes responsible for the housing roots of the teeth and are part of the periodontium complex. [8] The alveolar processes are composed of thin alveolar bone proper around the walls of the root sockets, cortical plates on buccal and lingual/palatal faces, and spongy bone between the cortical plates and the socket walls. All structures of the alveolar bone are developed and remodeled according to tooth formation and function, and therefore, are tooth-dependent bony structures. [8]

1.1.4 Long bones

Long bones are formed by endochondral ossification, which means ossification occurs by replacing a cartilage template. Two cartilage tissues play a role in long bone development, the growth plate and the articular cartilage. [9][10]

The long bone is divided into three zones: epiphysis, diaphysis, and metaphysis, also known as the growth plate. [9]] Long bone longitudinal growth occurs by cartilage being deposited at the epiphyseal side of the growth plate that is later mineralized. In the mature long bone, the remnant of the growth plate is present as an epiphyseal line. [9]

Appositional growth of the articular cartilage present in the knee joint occurs by chondrocyte proliferation in the superficial zone of the cartilage, which is replaced by collagen fibers that guide mineralization. [10]–[12]

1.2 Dentin

1.2.1 Composition

Dentin follows a similar structure pattern as bone, including mainly being composed of HA crystals. When comparing bone and dentin, the main difference is the

concentration of inorganic matter, where dentin is composed of 70% inorganic compared to 60% in the bone. In dentin, organic matter makes up 20% of its structure, comprising 90% collagen and 5 to 10% NCPs. [2]. Dentin composition is illustrated in figure 1.3.

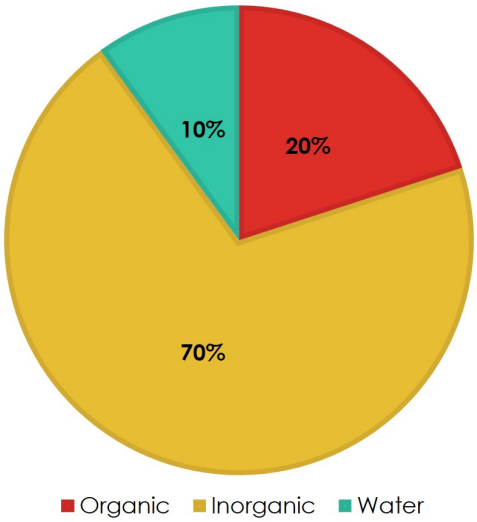

Figure 1.3: Dentin composition.

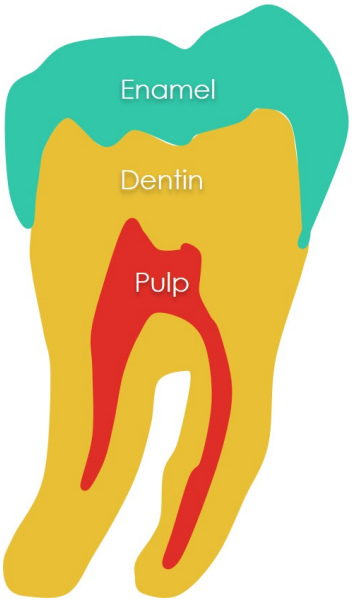

Figure 1.4: Tooth structure. Dentin accounts for the majority of the tooth structure, supporting the enamel while protecting the pulp.

1.2.2 Formation

Teeth are formed of enamel, dentin, and pulp, as illustrated in figure 1.4. Tooth and periodontium structures are developed from interactions between the oral ectoderm and mesenchymal cells derived from neural crest cells. [13]

There are four stages of tooth development: bud stage, cap stage, early bell stage, and late bell stage. [14][15] Dental hard tissue formation starts at the bell stage, and the most prominent cells that govern this process are odontoblasts and ameloblasts. [14][15] Odontoblasts are responsible for dentin production and are originated from mesenchymal cells adjacent to the dental epithelium. Ameloblasts are responsible for enamel production and are originated from inner enamel epithelium cells. [13]

Dentinogenesis is the process of dentin formation, where odontoblasts cease division to begin the secretory stage. Characteristic Tomes fibers elongate from odontoblasts to begin secretion of predentin, the initial organic matrix composed of collagens, proteoglycans, and glycoproteins. When predentin is approximately 5 to 10 microns thick, spherical crystallizing centers of HA growth are formed. [13][16] These globular dentin mineralization centers, called calcospherites, will fuse to form mineralized dentin. The initial layer of dentin is named mantle dentin, and the later mineralized part is named circumpulpal dentin. [13][16] Throughout dentin deposition, odontoblasts move towards the dental papilla, leaving an elongated process behind named the odontoblast process, which is surrounded by dentinal tubules. [13][16]

1.2.3 Bone and Dentin similarities

This study analyzes samples of bone and dentin. Bone and dentin are comparable tissues because they are developed from mesenchymal stem cells originating from the neural crest cells. [17][18] While dentin is formed by odontoblasts secreting predentin that is later mineralized,[19] bone is formed by osteoblasts secreting osteoid that is

later mineralized. [20]

Predentin and osteoid are precursors of their corresponding mineralized tissues. In their unmineralized phases, they lie between the mineralizing front and their depositing cells and are transformed in their mineralized phase as HA crystals are deposited. The biomineralization process involves multiple interactions between different molecules, among those, are type I collagen and NCPs. [17][19]

1.3 Non-Collagenous Proteins

NCPs are known to be regulators of mineralization of collagen fibers and crystal growth in predentin and osteoid when these tissues are being converted to dentin and bone. NCPs accounts for 5 to 10% of the bone and dentin organic component. NCPs play a role in regulating bone and dentin mineralization processes. [21]

1.3.1 SIBLING Family

The small integrin-binding ligand n-glycosylated (SIBLING) family is a category of NCPs. [22] This family includes dentin matrix protein 1 (DMP1), osteopontin (OPN), bone sialoprotein (BSP), and dentin sialophosphoprotein (DSPP). These proteins are all located on chromosome 4 in humans and this family shares a role in regulating function in mineralization and interactions with hydroxyapatite, which is the matrix of teeth and bone mineral structure. [22]

Another common feature of the SIBLING family members is that they all undergo the same post-translational modification (PTM), an enzymatic modification (phosphate regulating endopeptidase homolog X-linked enzyme) of the protein following synthesis. [23][22]

DMP1 protein is a product of chondrocytes and osteocytes, and it is not usually found in its intact form but rather in one of its cleaved products, an N-terminal pep-

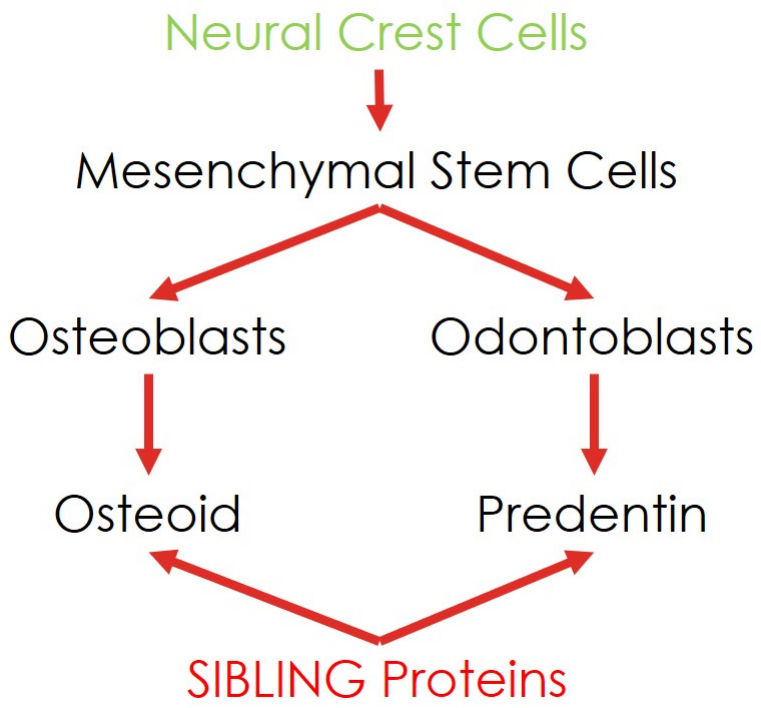

Figure 1.5: SIBLING proteins act in the mineralization of both osteoid and predentin. Playing a role in the formation of both bone and dentin.

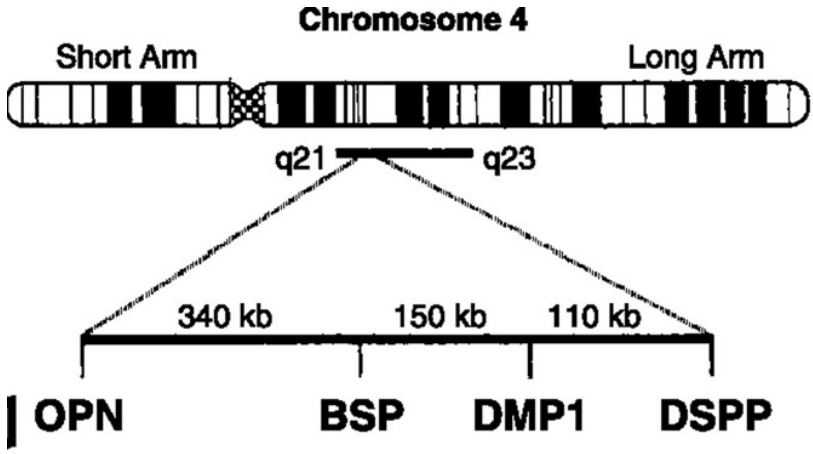

Figure 1.6: Chromosome 4 in humans. Adapted from Rodrigues et al. [24]

tide, a C-terminal peptide, and a glycosylated N-terminal protein. The intact protein and its glycosylated forms appear to inhibit mineralization, but the phosphorylated cleaved fragments can promote mineralization. [25]

OPN protein is the most abundant SIBLING protein. OPN is an inhibitor of mineralization, and when it is highly phosphorylated, it can promote hydroxyapatite formation. OPN is also involved in the recruitment of osteoclasts and in regulating the immune response. [26]

BSP protein is mostly expressed in bone-forming cells, with lower expression levels in other mineralized tissues such as dentin. [27][28] BSP is a hydroxyapatite nucleator, it facilitates osteoblast differentiation and maturation, therefore, stimulating mineralization. [29]

1.3.2 Dentin Sialophosphoprotein

DSPP was first sequenced and mapped in 1997 from the cloning of complementary deoxyribonucleic acid (DNA). [30] DSPP is a precursor protein that undergoes PTM to give rise to two proteins: dentin phosphoprotein (DPP) (COOH terminal fragment) and dentin sialoprotein (DSP) (NH2 terminal fragment). [31][32] In 1967 it was discovered that the most abundant NCP in the dentin extracellular matrix (ECM) is DPP, and in 1981 DSP was discovered as the second most abundant NCP in dentin ECM. [31][32] The DSPP gene contains five exons which encode a final part of the mRNA after introns are removed. [33]

During development, DSPP plays an important role in the formation of dentin, or dentinogenesis. [34]–[36] Dentinogenesis is a result of multiple protein signaling, and DSP has been indicated as a regulator of the initiation of dentin mineralization. [33] Meanwhile, DPP has been indicated to be an initiator and modulator in the formation and maturation of HA Crystals. [33]

Humans with defective DSPP gene express a severe dentin hypomineralization phenotype, a condition known as dentinogenesis imperfecta (DGI). [34]–[38] This condition causes the teeth to be discolored and translucent, a phenotype also known as

opalescent teeth. Teeth are also weaker than normal, prone to rapid wear, breakage, and loss. This condition can affect both primary teeth and permanent teeth. [39], [40] DGI affects approximately 1 in 6 000 to 8 000 people. Animal studies revealed that DSPP knockout (KO) mice manifest hypomineralization defects in dentin, resembling the dentin defects of human DGI. [34]–[36] A single copy of the altered gene is necessary to cause the disorder as an autosomal dominant condition. [39], [40]

According to the Shields classification system, DGI has historically been divided into three types.[40] DGI-I was a syndromic type associated with osteogenesis imperfecta, a genetic, developmental disorder in which all bones are brittle and prone to fracture.[41] Dental anomalies in the Shields DGI-I are associated with mutations in the COL1A1 and COL1A2 genes, and therefore, osteogenesis imperfecta with dental defects is currently considered a separate condition from DGI.[42] The types historically designated as DGI-II and DGI-III were non-syndromic and associated with mutations in the DSPP gene.

The most recent classification, the Mendelian Inheritance of Man (MIM) database, only divides DGI into two types.[38], [42], [43] The MIM database removed the Shields DGI-I from the list of DGI, and nowadays Shields DGI-I is classified as osteogenesis imperfecta.[42] Definitions of DGI-II and DGI-III were kept, and the MIM renamed DGI-II to DGI-I. Therefore, current classification divides DGI into DGI-I and DGI-III. DGI-I phenotype consists of opalescent teeth, as previously described.[44] DGI-III phenotype is described as "shell teeth", due to its radiographic appearance of notably large pulp chambers. [45]

DSPP gene mutations are also related to one type of dentin dysplasia (DD), which has the same symptoms as DGI, affecting dentin development, but mainly affecting primary teeth. [46]–[48] DD is classified as either Type 1 or Type 2. Type 1 is known as radicular DD and only affects root dentin. Type 2, also known as coronal DD,

affects the crown structure. DD affects approximately 1 in 100 000 individuals. [46], [47]DSPP mutation is associated with DD-II. [42]

Figure 1.7: DGI Type II. Adapted from Andersson et al. [49]

1.4 Recent findings

At first, DSPP was thought to be active only during dentinogenesis. This protein, however, has been identified in several other tissues such as bone, cementum, and several non-mineralized tissues, such as salivary glands, cartilage, liver, lung, kidney, and brain. [50]–[55] For example, in the long bone, DSPP is present at a lower expression level than in teeth. [54] Therefore, in mice models, DSPP defects express milder defects in the long bone than in teeth. [56] DSPP is also present in the mandibular condylar cartilage (MCC), located on the mandibular condyle and responsible for mandibular growth, but at a higher expression than in the long bone. [54] Despite its higher expression level, there have been no reports regarding the comparison of the expression pattern and phenotypic changes in the condylar cartilage of mice that do not express DSPP during development.

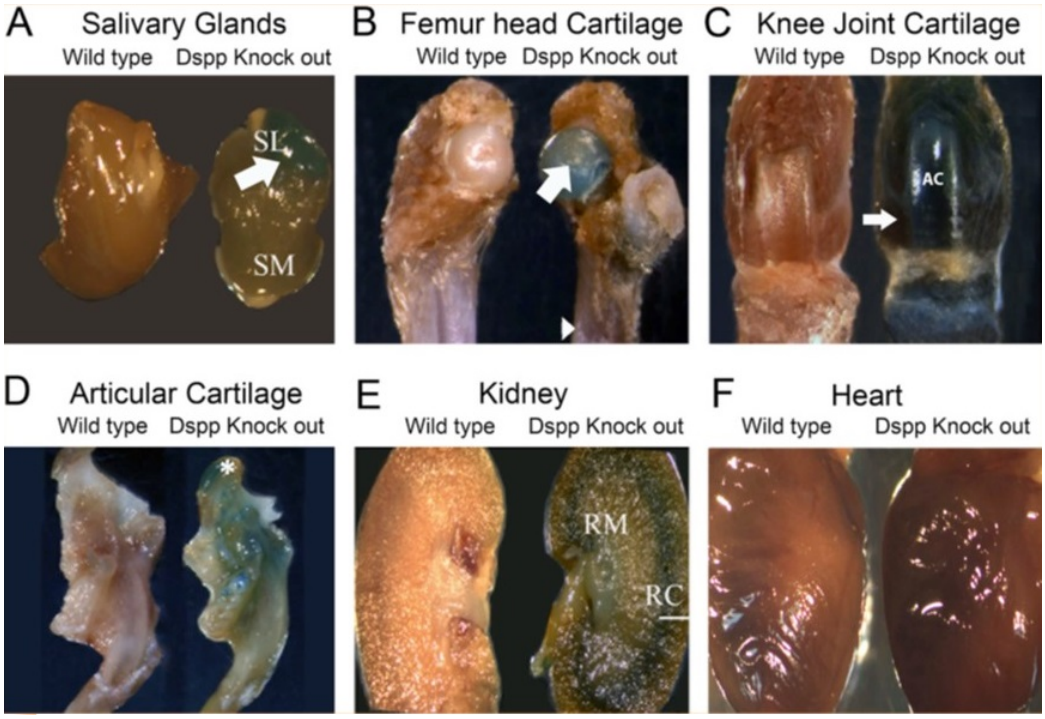

Figure 1.8: Lac-Z staining shows regions where DSPP is expressed in different tissues. Adapted from Gibson et al. [54]

1.4.1 Temporomandibular joint

The temporomandibular joint (TMJ) has unique features that differentiate it from other articulating joints in the body and is responsible for mastication and verbal communication. [57] The mandibular condyle is covered in fibrocartilage. [58] This fibrocartilage, named mandibular condylar cartilage (MCC) is secondary cartilage with a unique origin, cell differentiation and proliferation, and synthesis of ECM. [59][60] The MCC is derived from the periosteum after intramembranous bone formation and formed by progenitor cells derived from the neural crest. [60]

The MCC is composed of chondrocytes and ECM made of water, collagen, and proteoglycans, with other NCP and glycoproteins in smaller amounts. [61] Chondrocytes function in the ECM to synthesize and maintain the matrix under normal conditions, and the ECM is responsible for preserving the cartilage tissue integrity. [57]

1.4.2 Craniofacial structure

The bones from the craniofacial structure are originated from neural crest cells and mesodermal cells. Most of the bone, cartilage, and connective tissue from this structure is derived from the neural crest, including the odontoblasts, which, as mentioned before, secrete dentin. [62] DSPP is expressed in the connective tissues of the craniofacial complex with high expression levels in the ECM. But, similar to the MCC case, there is not much information regarding the expression and role of DSPP in the craniofacial complex. [63][64]

The calvaria development occurs via intramembranous ossification, meaning the mesenchymal stem cells differentiate directly into osteoblasts. In this type of ossification, mesenchymal stem cells form centers of ossification in which they differentiate into osteoblasts. [62] During development, the sutures between the calvarium bones serve as mesenchymal stem cell reserves for further ossification. This process is a result of an interplay between type I collagen matrix and the NCPs in the ECM. [62]–[64]

1.5 Objective

According to previous literature, we hypothesized that the knockout of DSPP would cause mineralization defects in the alveolar bone, skull, and mandibular condyle during development.

To address the gaps of knowledge stated in the recent findings section of the introduction, we formulated the research question: What are the impacts of knocking out DSPP in craniofacial development and long bone development in mice? For this research question, we will be investigating DSPP's expression and phenotypic changes in DSPP-/- mice in mandible development, calvarium growth, and long bone articular cartilage development.

Chapter 2

Materials and Methods

2.1 Experimental Mice

To analyze the role of DSPP in craniofacial development, two mice strains were used. DSPP-/- (strain name: B6; 129- *Dspp*$^{\mathrm{tm1Kul}}$/Mmnc;catalogue number 000047-UNC, MMRRC, UNC, North Carolina, USA) and Wild Type (C57BL/6J) mice from the Jackson Laboratory (Maine, USA) were compared. The development of the knockout strain has been previously described.[65] The comparison with the C57BL/6J control has been recommended by the manufacturer and published extensively in the literature. [48], [56], [66]–[69] The animal protocol has been approved by the Animal Care and Committee at the of Alberta (Study ID AUP00002086).

2.2 Breeding and Genotyping

Heterozygous mice for DSPP KO (DSPP+/-) were ordered and bred to generate pure homozygous for DSPP KO (DSPP-/-). Offspring were sacrificed with carbon dioxide (CO_2) at ages 1, 3, and 6 months. Genotyping of ear notch samples was used to confirm genotypes of the mice offspring. After ear notch samples were acquired, they were added to an Eppendorf tube (catalogue number 14-282-300, Thermo Fisher Scientific, Massachusetts, USA) with 300 microliters (µl) of electrolyzed total solution (ETS) and 5 µl of proteinase K (catalogue number AM2548, Thermo Fisher Scientific, Massachusetts, USA). Samples were then left overnight in the hot shaker (Bellco Glass

Inc., New Jersey, USA) water bath at 55 degrees Celsius (°C) and shaking speed set to 2.

Following lysis, the DNA was purified. After removing samples from the water bath and visually checking if lysing was completed, samples were vortexed for 30 seconds. 220 µl of the original solution were removed and added to 220 µl of phenol. Samples were then vortexed for 30 seconds and centrifuged at 15 000 rotations per minute (RPM) for 5 minutes at 24 °C. Supernatant was then removed (100 µl), and together with an equal amount of chloroform (100 µl), the new solution was added to new Eppendorf tubes. The supernatant and chloroform solution was vortexed for 30 seconds and centrifuged at 15 000 RPM for 5 minutes at 24 °C. Supernatant was removed from the latest solution (100 µl) and, together with 200 µl of ethanol, were added to final Eppendorf tubes. The final solution was centrifuged at 15 000 RPM for 5 minutes at 4 °C, and finally, after this step, DNA pellets were visible at the bottom of the solution. The 300 µl of solution were then removed from the tubes, and the DNA pellets left to dry overnight.

The next step was the polymerase chain reaction (PCR). Before starting PCR, DNA concentration was checked on NanoDrop 2000c (Thermo Fisher Scientific, Massachusetts, USA). For that, 50 µl of 1x Tris-EDTA (TE) were added to the DNA tubes, then 1 µl of the solution was added to the NanoDrop 2000c machine. PCR mixes contained 23 µl of Taq polymerase solution and 2 µl of DNA solutions from each sample. The Taq polymerase solution was composed of 12.5 µl of Taq polymerase (catalogue number 10342053, Thermo Fisher Scientific, Massachusetts, USA), 11 µl of distilled water, and 0.5 µl each of forward, reverse, and LacZ primers (6.5% of total solution) (Primer sequences 5' to 3': DsppFOR1: GTATCTTCATGGCTGTTGCTTC DsppREV1: TGTGTTTGCCTTCATCGAGA LacZREV1: CCTCTTCGCTATTACGCCAG). The negative control used was water, and the positive control was heterozygous DNA.

We then proceeded to the PCR machine (T100 thermal cycler, Bio-Rad Laboratories, California, USA). PCR protocol was as follows. Step 1: 5 minutes at 94 °C. Step 2: 45 seconds at 94 °C. Step 3: 45 seconds at 56 °C. Step 4: 1 minute at 72 °C. Step 5: go to step 2 and repeat 36 times. Step 6: 7 minutes at 72 °C.

After PCR, we proceeded to gel electrophoresis. Agarose gel was prepared with 3 grams of agarose (catalogue number 16500100, Thermo Fisher Scientific, Massachusetts, USA) and 150 ml of tris-acetate-EDTA (TAE) (catalogue number 15558042, Thermo Fisher Scientific, Massachusetts, USA). This solution was microwaved for 2 minutes, and then 5 µl of ethidium bromide (catalogue number 15585011 Thermo Fisher Scientific, Massachusetts, USA) were added. Gel running buffer was composed of 1 liter of 1x TAE. After placing gel and running buffer in the DNA electrophoresis system (Bio-Rad Wide Mini-Sub Cell GT, Bio-Rad Laboratories, California, USA), 5 µl of DNA ladder were loaded, followed by 20 µl of each DNA samples and controls. The gel was run at 250 volts, 0.1 ampers and 290 watts for 40 minutes, with the PowerPac HC power supply (Bio-Rad Laboratories, California, USA). The gel was then placed in the ChemiDoc MP imaging system (Bio-Rad Laboratories, California, USA). Results are shown in figure2.2.

2.3 Sample preparation

Long bones, skulls, and hemi-mandibles were surgically removed from mice post-mortem. Samples were subdivided and stored according to the analysis procedure. A total of 180 samples were cleaned and prepared. Two groups of samples divided into 5 for each genotype in each age group were created. One group was used for morphological analysis, therefore those were fixed in 4% paraformaldehyde (PFA). Another group was used for histological analysis, therefore those were fixed in 4% PFA and decalcified in 8% ethylenediaminetetraacetic acid (EDTA).

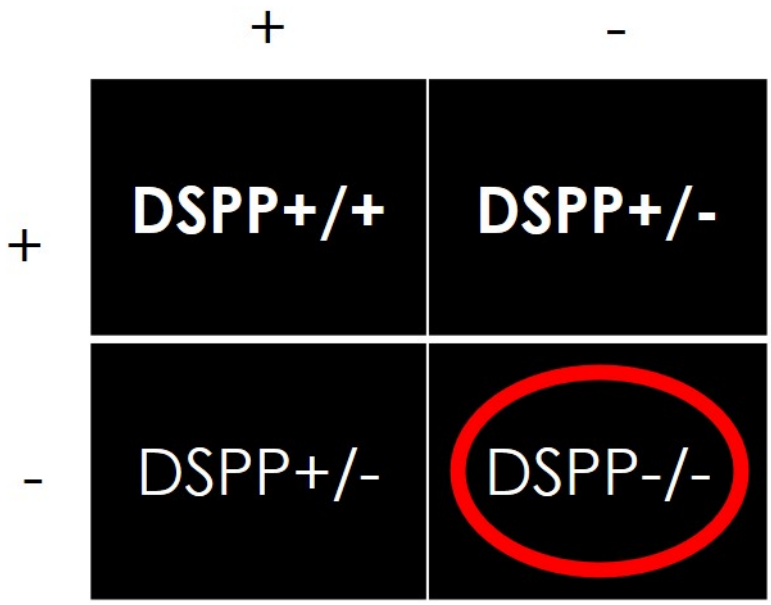

Figure 2.1: Heterozygous breeding outcomes

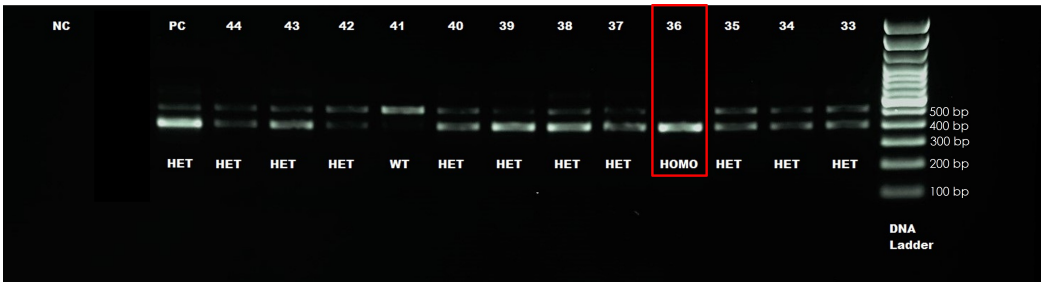

Figure 2.2: Example of gel electrophoresis DNA results. WT allele bands have 489bp compared to 389bp on homozygous for KO.(NC stands for negative control, PC stands for positive control, HET stands for heterozygous, WT stands for wild type, and HOMO stands for homozygous.)

2.4 Radiographic analysis

Long bones, skulls, and hemi-mandibles samples were imaged by high-resolution digital radiography (Faxitron model UltraFocus DXA; Faxitron Bioptics, Arizona, USA). Samples were placed on the magnification tray at position 5, and the detection tray was positioned at the base of the machine, according to manufacturer recommendations. Faxitron Vision software was used to analyze results.

2.5 Dual-Energy X-Ray Absorptiometry

Faxtiron (modelUltraFocus DXA; Faxitron Bioptics, Arizona, USA) Dual-energy x-ray absorptiometry (DXA) system was used to measure BMD in regions of interest (ROIs). Samples and detection tray were placed at position 2 of the machine, according to manufacturer recommendations. DXA Vision software (Faxitron Bioptics, Arizona, USA) was used to extract BMD results from the scans.

2.6 Selection of ROIs

The Faxitron Vision software yields six different images when a sample is scanned. Those are bone map, DXA map, lean map, fat map, low energy x-ray, and high energy x-ray. The selection of ROIs was made in the low-energy image, as recommended by the manufacturer, to allow better distinction between soft and hard tissues.

Faxitron vision allows the selection of regions of interest with a freely drawn rectangular shape or free shape. Extensive research was conducted prior to the selection of regions of interest, and rectangular regions of interest were selected according to previous literature. [70]–[76] A recent systematic review described the regions of interest of 42 studies that analyzed rodent jaw bone with micro-CT. This review mentions that many studies do not make it clear in their methodology how the ROI was selected, and there is a lot of variation between regions of interest selected in rodent mandibles.[76] The ROI for molars and condyles was selected according to a recent study which analyzed rodent jawbone microstructure with micro-CT. [71]

The ROIs in long bones were selected according to a recent paper that analyzed BMD in long bones with DXA.[77] The region of interest for the skull was selected according to previous literature that analyzed BMD in the calvaria.[78], [79] ROI for condyles followed previous literature which analyzed BMD in the mandibular condyle of rats with micro-CT. [80]

Therefore, two ROIs for bone mineral density measurement were selected on mandible samples: molars and mandibular condylar cartilage. In long bone samples, an ROI was selected at the edge of the distal femur condyle. In skulls, an ROI for BMD analysis was selected involving the calvaria region. Regions of interest were the same size for all samples and are illustrated in figures 2.3, 2.4, and 2.5.

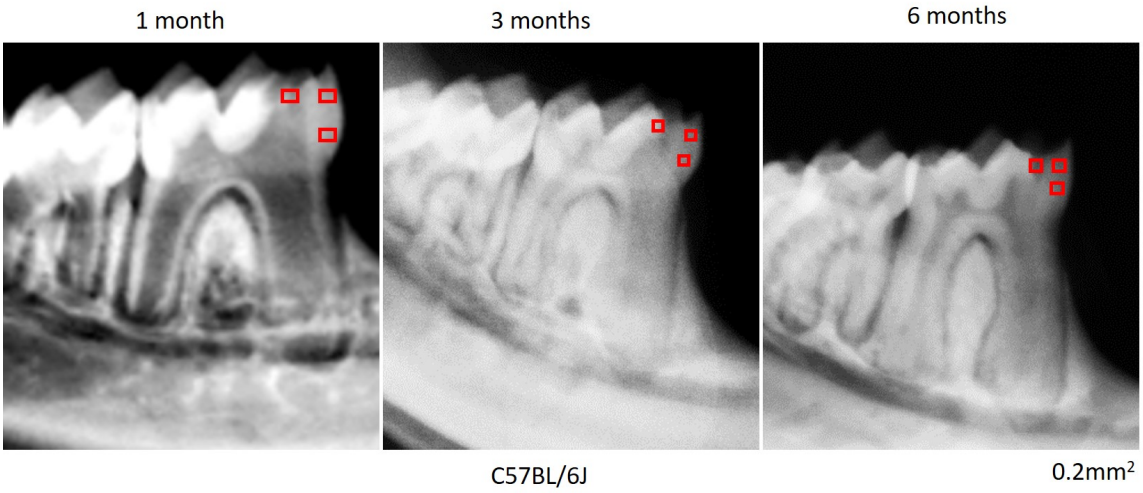

Figure 2.3: Selected regions of interest in dentin in the three age groups. Box size: $0.2mm^2$

2.7 Micro-computed Tomography (micro-CT)

Three-dimensional micro-CT scans of dissected hemi-mandibles, skulls, and long bones were taken at 360°, 75 milliseconds, 50 kilovolts, and 0.24 milliamps (Milabs U-CT, Utrecht, Netherlands). Scans were reconstructed in MiLabs Software at 25 micrometers voxel size and analyzed with Amira software (ThermoFisher Scientific, Ontario, Canada).

2.8 Cell Culture

Cell culture was done according to Chen et al.[81]. Primary calvaria cells were extracted from calvaria of 1-month-old C57BL/6J and DSPP-/- mice. Mice were euthanized with CO_2, and the protocol immediately proceeded to avoid loss of cell

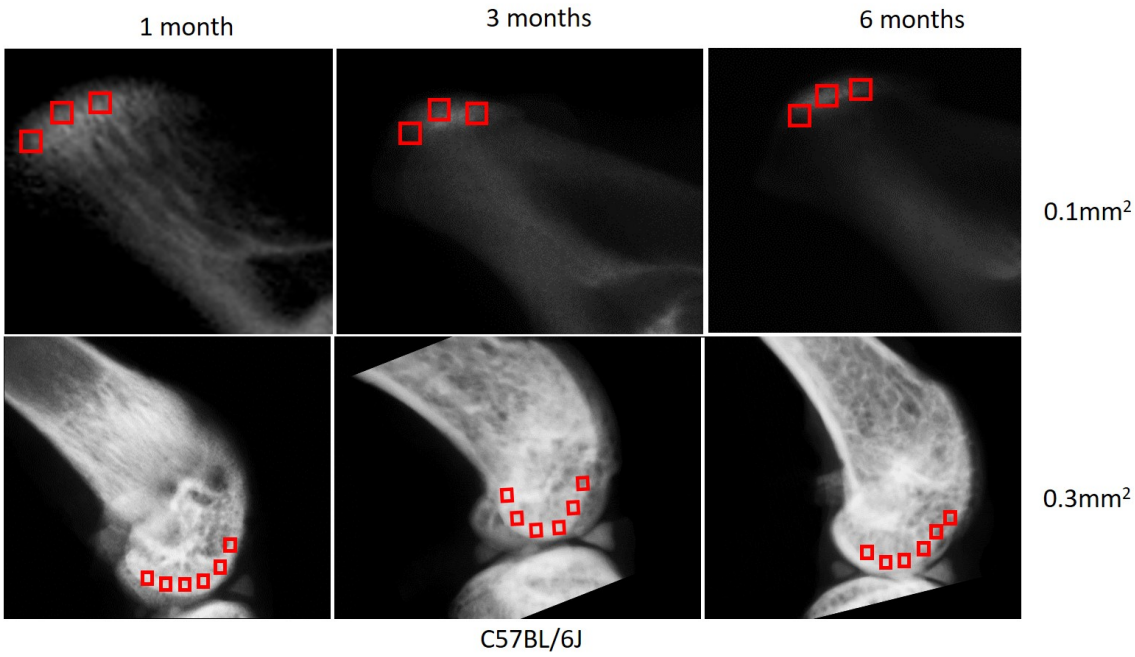

Figure 2.4: Selected regions of interest in mandibular and long bone condyles in the three age groups.Box sizes: $0.1mm^2$ for mandibular condyle and $0.3mm^3$ for long bone condyle

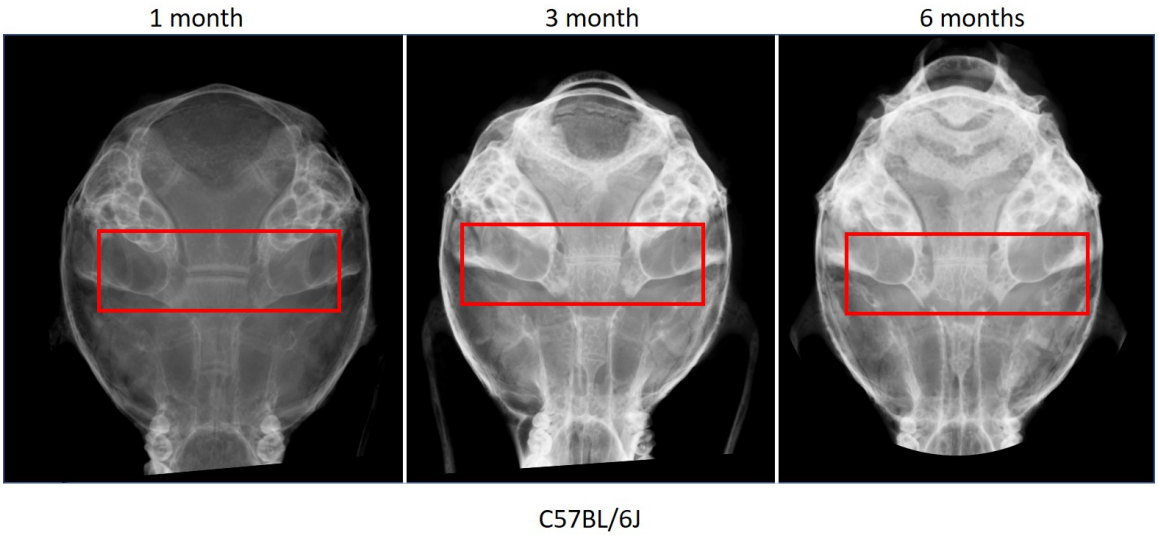

Figure 2.5: Selected regions of interest in skulls in the three age groups.

viability. All steps were carried out in Class II biological safety cabinet using sterile technique. Parietal bones were placed in a petri dish with sterile phosphate-buffered saline (PBS) (catalogue number BP3994, Thermo Fisher, Massachusetts,

USA) and cleaned. Calvaria was transferred to a sterile specimen cup and isolated by a sequential enzymatic digestion cocktail containing collagenase (catalogue number 11213857001, Millipore Sigma, Massachusetts, USA) and PBS in a concentration of 1.5 units of collagenase per mL of PBS, 0.05% trypsin (catalogue number 650277, Millipore Sigma, Burlington, Massachusetts, USA) and 0.2 millimole EDTA (catalogue number 15576028, Thermo Fisher Scientific, Massachusetts, USA). Cells were filtered through a sterile 70 microns nylon cell strainer, pelleted, and culture in Dulbecco's modified eagle medium (catalogue number D5546-500ML, Millipore Sigma, Massachusetts, USA) with 10% fetal bovine serum and 1% antibiotic-antimycotic solution (catalogue number 15240062, Thermo Fisher Scientific, Massachusetts, USA) in sterile 75 square centimeters flasks (catalogue number 156472, Thermo Fisher Scientific, Massachusetts, USA).

Osteoblast differentiation ***in vitro*** is divided into 3 stages, cell proliferation, matrix maturation, and matrix mineralization. Matrix maturation and mineralization are enhanced by growing the cells to complete confluency and by adding specific osteogenic factors (10 mM B-glycerophosphate [catalogue number G9422, Millipore Sigma, Massachusetts, USA], 0.2 mg/ml ascorbic acid [catalogue number A4544, Millipore Sigma, Massachusetts, USA], and 10 nanomoles dexamethasone [catalogue number D4902, Millipore Sigma, Massachusetts, USA]). Culture media was changed twice a week for up to 3 weeks. Cells were cultured to 70–80% confluence before passaging. Artificial growth conditions in the incubator were 37 °C and 5% CO_2.

Media change was conducted using sterile technique as previously described. Cells were rinsed with PBS, and cell dissociation solution (trypsin) was added to detach the cells from the flasks. The cells were transferred to a conical tube and centrifuged at 1000 RPM for 10 minutes to form a pellet. The medium was discarded. The pellet was resuspended with new growth medium, and the solution was added to 35 mil-

limeters tissue culture dishes (catalogue number 12556000, Thermo Fisher Scientific, Massachusetts, USA). Cells were examined under the microscope for counting and viability, making sure cells were attached to the dishes and not floating.

2.9 Alizarin Red Staining

To visualize calcium deposits in cell culture, the cells were fixed with 1ml 10% formaldehyde for 10 minutes at room temperature (RT) and washed with 1.5 ml PBS twice, and then stained with 1ml 2% alizarin red s (catalogue number A5533, Millipore Sigma, Massachusetts, USA) solution for 15 minutes at RT. Lastly, cells were fully washed with double distilled water and observed under a microscope.

2.10 Hematoxylin & Eosin (H&E) Staining

H&E staining was used to analyze different histological features of DSPP-/- and C57BL/6J samples. Dissected skulls, long bones, and hemi-mandibles selected for histological analysis were decalcified in EDTA 8% before paraffin embedding. Samples were embedded by the University of Alberta HistoCore. Skulls were embedded in an anterior-posterior orientation. Hemi-mandibles and long bones were embedded in a medial-lateral orientation. Blocks were cut into 5-micron sections parallel to the surfaces of the blocks with a Leica HistoCore Autocut microtome (Leica, Wetzlar, Germany). Mandibles and long bones were cut in a mesial-distal direction, and skulls were cut from the frontal view. Paraffin sections were immediately placed in a water bath at 35 °C and collected on to superfrost plus microscope slides (catalogue number 12-550-15, Thermo Fisher Scientific, Massachusetts, USA). Each slide contained 2 or 3 samples. Even slides were stained with H&E. Odd slides were used for immunohistochemistry (IHC) staining.

Deparaffinization, staining and mounting protocol were conducted as follows: Prior to deparaffinization, samples were left in a vacuum oven (Thermo Fisher Scientific,

Massachusetts, USA) at 37 °C overnight. Deparaffinization was conducted with two changes of xylene for 10 minutes. Then 100% ethanol (EtOH) was used with two changes for 5 minutes, 95% EtOH for 5 minutes and 70% EtOH for 2 minutes. Hematoxylin (Harris hematoxylin solution, catalogue number HHS32, Millipore Sigma, Massachusetts, USA) staining was then conducted for 3 minutes. Slides were then washed in running tap water for 5 minutes. Differentiation solution (catalogue number A3179, Millipore Sigma, Massachusetts, USA) was used next for 30 seconds. Samples were again washed in running tap water for 1 minute, and then Scott's tap water (catalogue number S5134, Millipore Sigma, Massachusetts, USA) was applied for 30 seconds. Following, samples were washed in running tap water for 1 minute, and eosin (catalogue number HT110332, Millipore Sigma, Massachusetts, USA) was applied for 30 seconds. Samples were then dehydrated with 95% EtOH for 3 minutes, two changes of 100% EtOH during 3 minutes and two changes of xylene during 3 minutes. After drying for 12 hours, Permount (catalogue number SP15100, Thermo Fisher Scientific, Massachusetts, USA) was used, and microscope cover glass (catalogue number 16004-312 VWR Avantor, Pennsylvania, USA) were applied to the slides. Staining results were finally observed under a Leica DMRE (Model DM2000, Leica, Wetzlar, Germany) microscope.

2.11 Immunohistochemistry (IHC) Staining

IHC staining was used to analyze the difference in expression of DSPP in DSPP-/- and C57BL/6J samples. IHC samples went through the same embedding and cutting protocol as the H&E samples.

The IHC protocol is as follows: Prior to deparaffinization, samples were left in a vacuum oven (Thermo Fisher Scientific, Massachusetts, USA) at 37 °C overnight. Deparaffinization was conducted with three changes of xylene for 10 minutes each. Then, three changes of 100% EtOH and one change of 100% methanol for 2 minutes were

used. Blocking with 0.3% H_2O_2 in 250 ml of methanol to inactivate endogenous peroxidase was then conducted. Next, samples were treated with hyaluronidase 1mg/ml in 0.01M PBS at 37 °C to expose epitopes of target proteins. Samples were then washed in PBS for 2 minutes and incubated overnight at 4 °C in 100 µl of mouse IgG blocking reagent (mouse on mouse blocking reagent, catalogue number MKB-2213-1, Vector Laboratories, California, USA) diluted into 2.5ml of PBS. The following day, samples were washed with PBS for 2 minutes and incubated for 5 minutes in 300 µl of protein concentrate (mouse on mouse immunodetection kit, catalogue number PK-2200, Vector Laboratories, California, USA) diluted in 3.75 ml of PBS. Samples were then incubated with anti-DSP monoclonal antibody (anti-DSP-2C12.3 Monoclonal – MABT37, EMD Millipore) at a 1:800 dilution in the protein concentrate and PBS solution previously described. Samples were then washed with PBS for 5 minutes and, as a negative control, incubated for 30 minutes with the secondary antibody, 5 µl of biotinylated anti-mouse immunoglobulin G (mouse on mouse immunodetection kit, catalogue number PK-2200, Vector Laboratories, California, USA) diluted in the protein concentrate and PBS solution previously described. Next, samples were washed with PBS for 5 minutes and treated with the avidin-biotin complex kit (catalogue number PK-6100, Vector Laboratories, California, USA). Next, samples were washed in PBS for 5 minutes and treated for 10 minutes with the 3,3' diaminobenzidine kit (catalogue number SK-4100, Vector Laboratories, California, USA) for color development. Protocols for preparation of the avidin-biotin complex kit and the 3,3' diaminobenzidine kit followed manufacturer instructions. After color development, samples were placed in distilled water for 30 seconds and counterstained with methyl green (catalogue number 67060-10g, Millipore Sigma, Burlington, Massachusetts, USA) solution for 30 seconds. Methyl green solution was composed of 1.75 ml of 5% methyl green in distilled water, 25 ml of 0.2 M acetate buffer (catalogue number 12950684, Thermo Fisher Scientific, Massachusetts, USA) at pH 4.7, and 25 ml of water.Slides were mounted with 50% glycerol (catalogue number G5516-

1L, Millipore Sigma, Massachusetts, USA) and covered with microscope cover glasses (catalogue number 16004-312 VWR Avantor, Pennsylvania, United States). Results were then immediately observed under the Leica DMRE (DM2000) microscope with a Leica MC170HD camera.

2.12 Image Capture

All IHC and H&E stained slides were visualized under the Leica DMRE (DM2000) microscope. A Leica MC170HD camera mounted on the microscope was used to capture all images. Image formatting settings were adjusted in the Leica application suite LASv4.9 software (Leica Microsystems; Wetzlar, Germany) to achieve background red, green and blue balance and white color balance. Images were captured with 5x, 10x, 20x, and 40x magnification depending on the region of interest. Cell culture images were captured with a Samsung camera (Model A51, Samsung Group; Seoul, South Korea).

2.13 Statistical Analysis

Microsoft Excel software (Microsoft Corporation; Redmond, Washington) was used to analyze bone mineral density results. The sample size was calculated based on power analysis of previous studies on dentin. [66], [82]–[85] Same number was applied for other tissues as there was no preceding data on the differences to calculate power. Therefore, a sample size of five was used for each age and each genotype, with the exception of the condyle that had a sample size of three for each. The Kolmogorov-Smirnov test was used to check the normality of our results. The paired T-test with two samples for means was used to check the significance of differences between DSPP-/- and C57BL/6J results. The alpha value was set to 0.05. Statistical significance was defined at p smaller than 0.05.

All descriptive results were assessed by three investigators, one of whom was blinded. The described results were true for all samples analyzed.

Chapter 3

Results

The present study aimed at investigating the impact of the DSPP protein absence in the mineralization process during development in mice. To investigate the role of DSPP in craniofacial development, C57BL/6J and DSPP-/- mice were compared at 1, 3, and 6 months of age using different methods.

3.1 X-ray results

UltraFocus DXA (Faxitron Bioptics, Tucson, AZ, USA) yielded high-resolution radiographic images used for morphological analyses of the samples under investigation.

3.1.1 Molars

Radiographic images of dental tissues from 1 month age group showed thinner dentin and enamel on DSPP-/- samples compared to C57BL/6J. Molars showed more radiolucency in DSPP-/- samples due to pulp enlargement. At 3 months of age, extensive destruction of the DSPP-/- first molar by cariogenic activity was noticed. Images from the 6 months-old group showed extensive destruction of the DSPP-/- second molar. Enlargement of the pulp can be noticed in the DSPP-/- image. (figure 3.1).

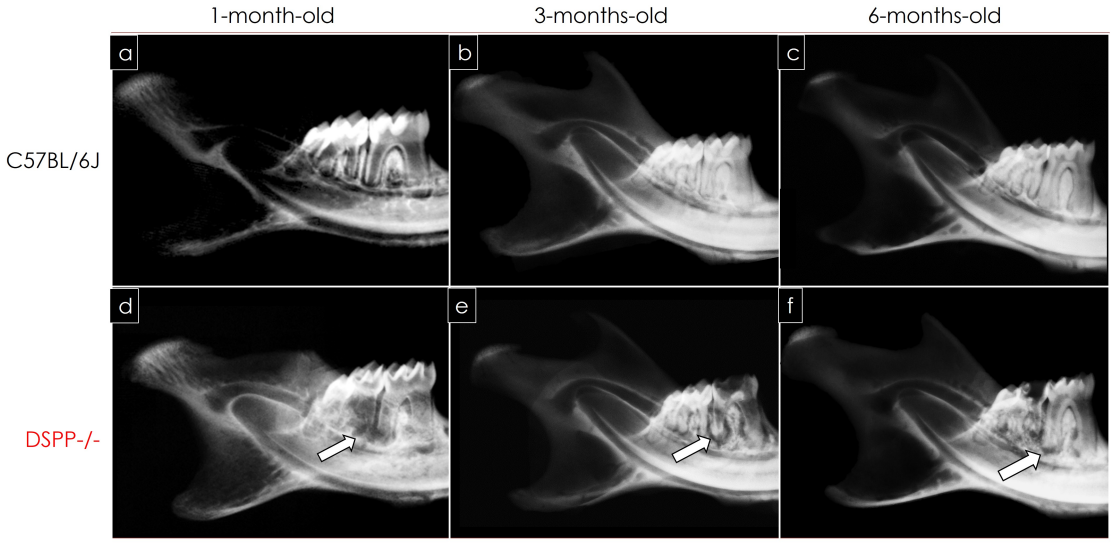

Figure 3.1: Radiographic images of 1, 3, and 6-months old mice mandibles. Figures 3.1(a-c) represent C57BL/6J mice, and figures 3.1 (d-f) represent DSPP-/- mice. Figure 3.1(a) shows thin enamel and dentin structures and an enlarged pulp chamber. Figure 3.1(d) shows a radiolucent region around the distal root of the first molar (white arrow). The head of the condyle is more radio-opaque in figure 3.1(d). Figure 3.1(e) shows demineralized dental tissues (white arrow) and thin condyle anatomy. Figure 3.1(f) shows less mineralized alveolar bone (white arrow) and less radio-opaque condylar process compared to figure 3.1(c).

3.1.2 Condyles

In mandibular tissues at 1 month of age DSPP-/- mice, radiographic images showed a more radio-opaque head of the condyle than C57BL/6J mice, most significantly detected in the articular surface. 3-month-old DSPP -/- images showed less radio-opaque condylar process compared to the C57BL/6J image. However, the articular cartilage region of the condyle has a similar appearance to the C57BL/6J image. At 6-months-old, the condylar process of the DSPP -/- mice showed less radiopacity than the C57BL/6J condylar process. (figures 3.1).

3.1.3 Skulls

Radiographic images of calvaria regions of skull samples did not show noticeable differences between DSPP-/- and C57BL/6J mice at 1, 3, or 6 months of age. (figure

3.2).

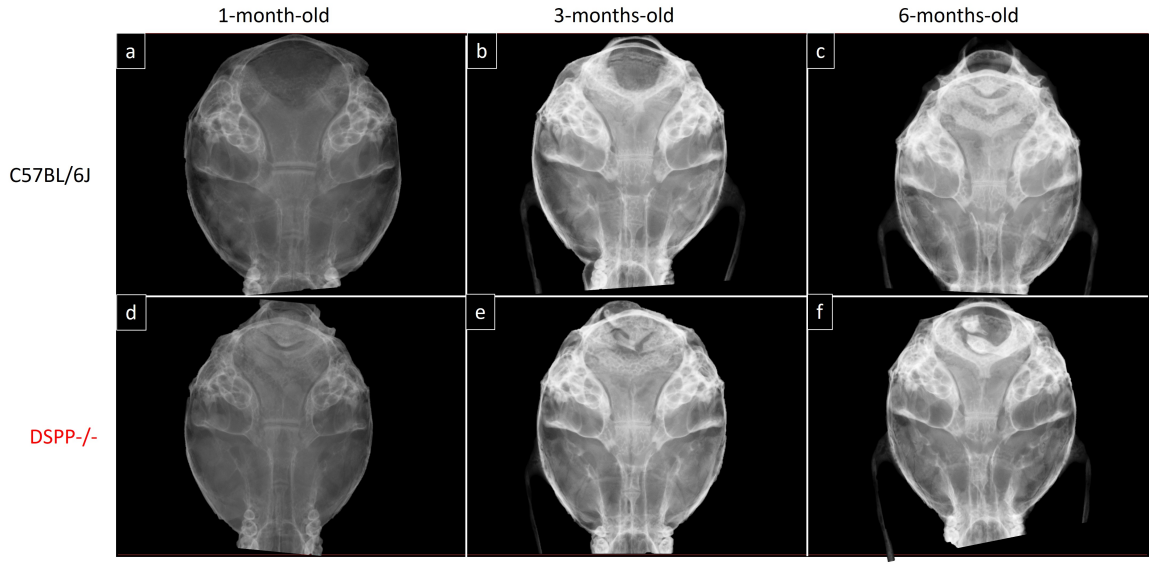

Figure 3.2: Radiographic images of 1, 3, and 6-months old mice skulls. Figures 3.2(a-c) represent C57BL/6J mice, and figures 3.2(d-f) represent DSPP-/- mice. No clear difference could be seen between C57BL/6J and DSPP -/- samples.

3.1.4 Long Bones

Radiographic images of 1-month-old long bones showed an enlarged growth plate in DSPP-/- samples compared to C57BL/6J. At 3 and 6 months of age, no clear difference could be noticed between DSPP-/- and C57BL/6J groups. (figure 3.3).

3.2 Faxitron DXA

3.2.1 Dentin

In C57BL/6J molars, for 1-, 3-, and 6-months-old samples, the BMD mean results were 89.35($\pm$1.34), 94.9($\pm$1.64), and 98.8($\pm$5.88), respectively. In DSPP-/- molars, for 1, 3, and 6 months of age, the BMD mean results were 60.98($\pm$8.05), 72.07($\pm$6.27), and 78.58($\pm$4.30). (Figure 3.4)

Figure 3.3: Radiographic images of 1, 3, and 6-months old mice long bones. Figures 3.3(a-c) represent C57BL/6J mice, and figures 3.2(d-f) represent DSPP-/- mice. Figure 3.3(d) shows an enlarged growth plate compared to 3.3(a). No other significant differences were observed between the other age groups.

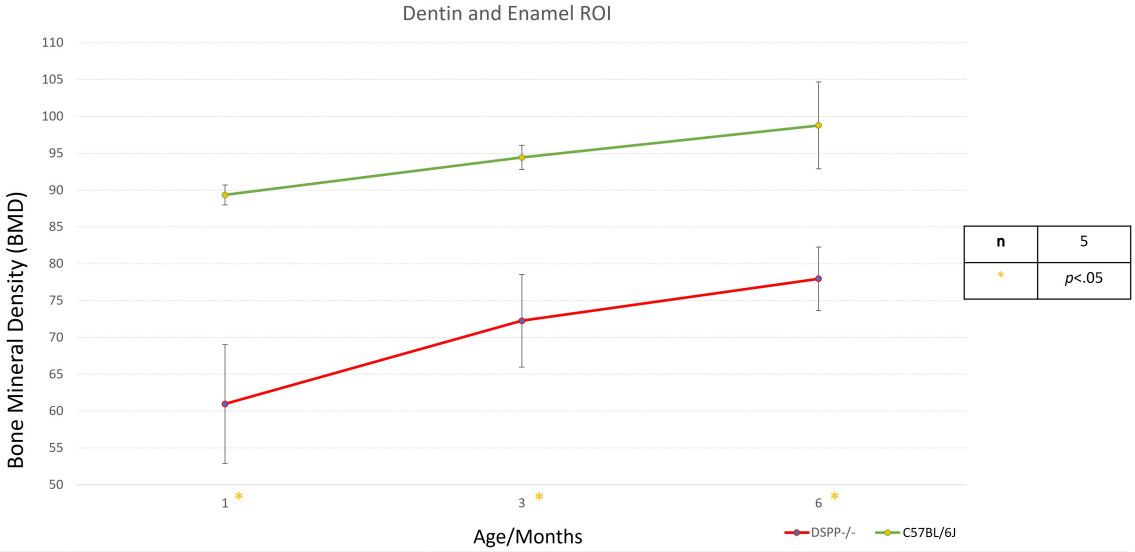

	1 Month			3 Months			6 Months		
	Mean BMD (mg/cm2)	SD	*p* value	Mean BMD (mg/cm2)	SD	*p* value	Mean BMD (mg/cm2)	SD	*p* value
C57BL/6J	89.355	1.343	0.003	94.976	1.651	0.001	98.816	5.888	0.001
DSPP-/-	60.986	8.059		72.074	6.273		78.582	4.305	

Figure 3.4: BMD results of 1, 3, and 6-months old C57BL/6J and DSPP-/- mice dentin and enamel ROI. The green line represents C57BL/6J mice red line represents DSPP-/- mice. C57BL/6J mice had higher BMD in all ages.

3.2.2 MCC

In C57BL/6J mandibular condylar cartilage, results for BMD means at 1, 3, and 6 months of age were 39.06(±3.32), 73.24(±6.21), and 74.13(±3.76), respectively. In DSPP-/- mandibular condylar cartilage, results for BMD means at 1, 3, and 6 months of age were 42.42(±3.50), 58.41(±5.03), and 69.26(±6.16), respectively. (Figure 3.5)

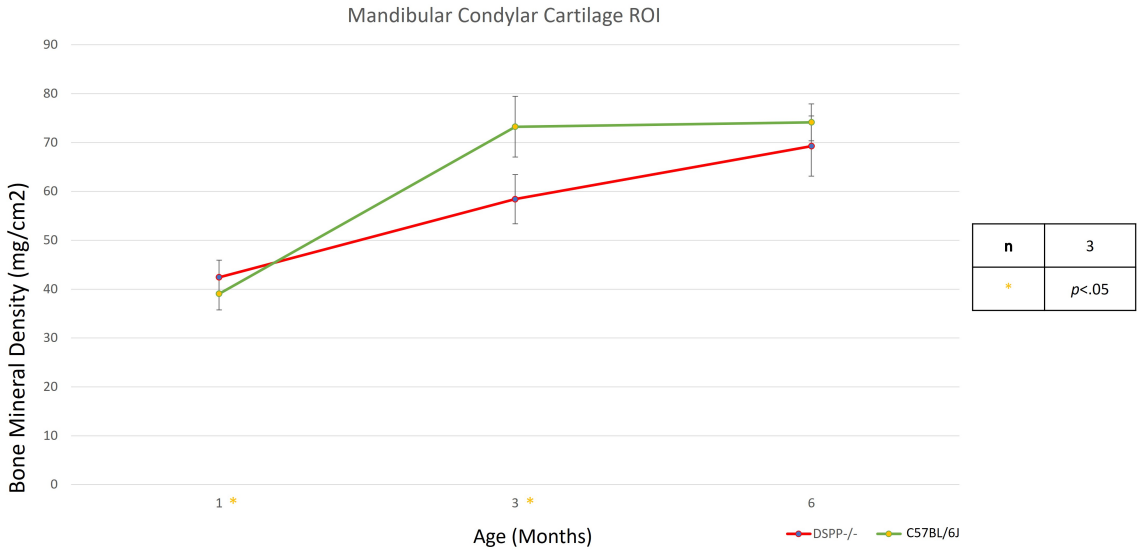

	1 Month			3 Months			6 Months		
	Mean BMD (mg/cm2)	SD	*p* value	Mean BMD (mg/cm2)	SD	*p* value	Mean BMD (mg/cm2)	SD	*p* value
C57BL/6J	39.0625	3.322695	0.012	73.24625	6.215	0.007	74.13775	3.763882	0.151
DSPP-/-	42.429	3.504421		58.41925	5.036		69.26775	6.167548	

Figure 3.5: BMD results of 1, 3, and 6-months old mice mandibular condylar cartilage ROI. The green line represents C57BL/6J mice red line represents DSPP-/- mice. DSPP-/- mice had higher BMD at 1 month of age. C57BL/6J showed higher BMD at 3 months of age. At 6 months of age, no statistically significant difference was shown.

3.2.3 Long Bone

C57BL/6J long bone BMD mean results at 1, 3, and 6 months of age were 98.50(±2.56), 166.81(±6.80), and 177.23(±22.22), respectively. DSPP-/- long bone BMD mean results at 1, 3, and 6 months of age were 88.12(±8.09), 142.35(±11.01), and 160.72(±17.26), respectively. (Figure 3.6)

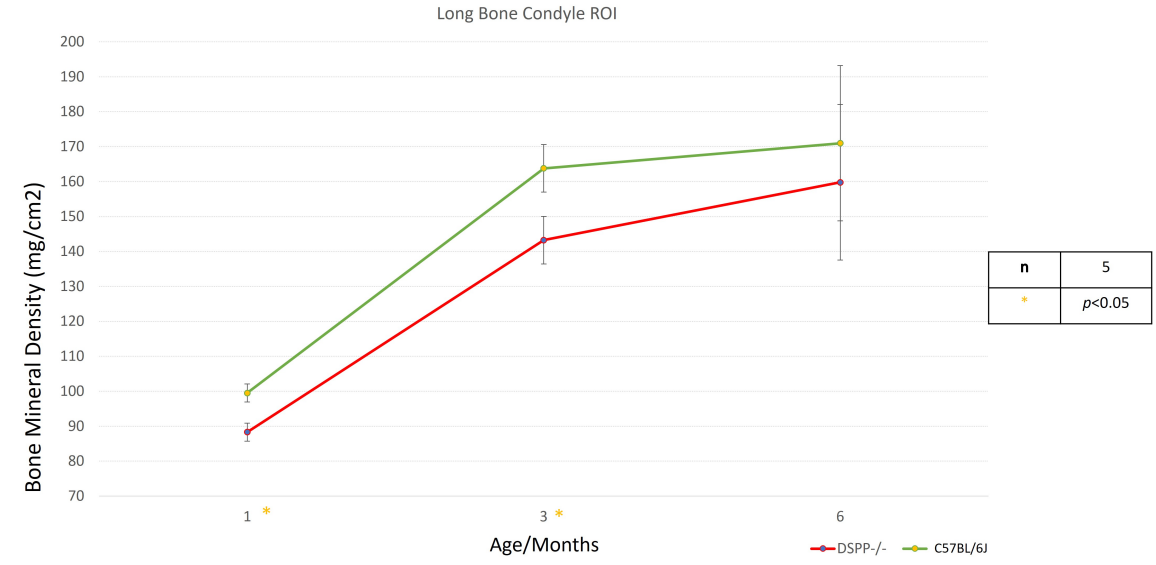

	1 Month			3 Months			6 Months		
	Mean BMD (mg/cm2)	SD	*p* value	Mean BMD (mg/cm2)	SD	*p* value	Mean BMD (mg/cm2)	SD	*p* value
C57BL/6J	98.50866667	2.567836703	0.043685	166.811	6.8056427	0.026936668	177.2315	22.22972	0.180939
DSPP-/-	88.12233333	8.095691776		142.3555	11.012316		160.72725	17.2665	

Figure 3.6: BMD results of 1, 3, and 6-months old mice long bone ROI. The green line represents C57BL/6J mice red line represents DSPP-/- mice. C57BL/6J mice had higher BMD in all age groups.

3.2.4 Skull

C57BL/6J skull BMD mean results at 1, 3, and 6 months of age were 46.73($\pm$1.9), 84.69($\pm$4.13), and 76.25($\pm$2.3), respectively. BMD mean results for DSPP -/- samples at 1, 3, and 6 months of age were 42.85($\pm$2.97), 72.38($\pm$5.05), and 75.79($\pm$4.45), respectively. (Figure 3.7)

3.3 Micro-Computed Tomography

Three-dimensional Micro-CT scans were used to compare bone structural surfaces between the C57BL/6J and DSPP-/- mice.

3.3.1 Alveolar Bone

At 1 month of age, severe demineralization can be noticed in the DSPP-/- alveolar bone. It showed a rough and porous architecture and evident demineralized zones exposing molar furcation areas. At 3-months-old, the difference between the two

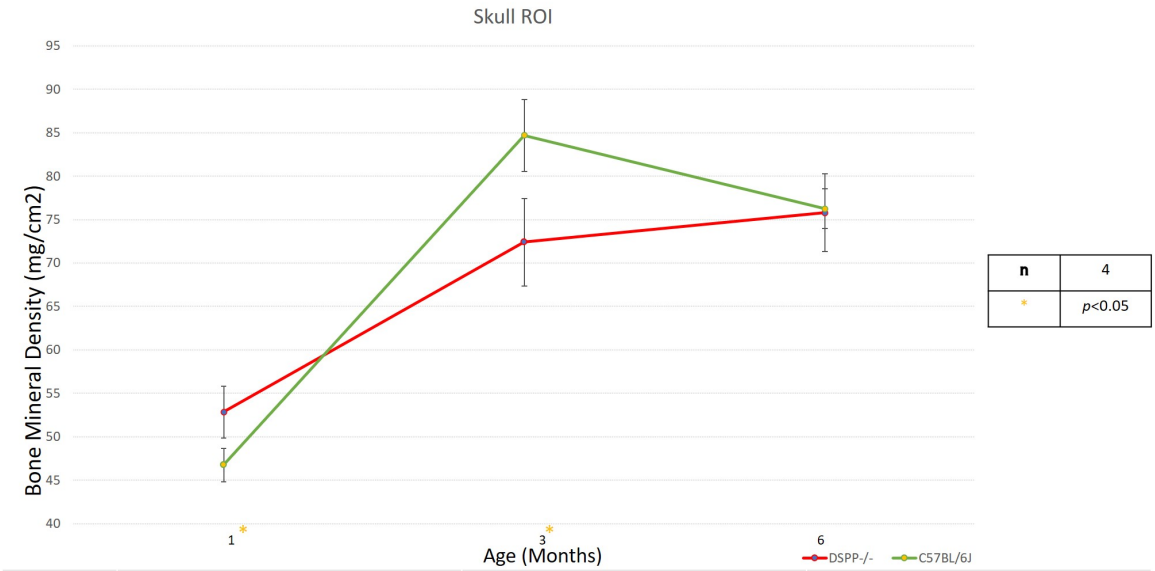

	1 Month			3 Months			6 Months		
	Mean BMD (mg/cm2)	SD	p value	Mean BMD (mg/cm2)	SD	p value	Mean BMD (mg/cm2)	SD	p value
C57BL/6J	46.736	1.904	0.005	84.699	4.136	0.003	76.258	2.3	0.436
DSPP-/-	52.853	2.974		72.387	5.058		75.795	4.452	

Figure 3.7: BMD results of 1, 3, and 6-months old mice skull ROI. The green line represents C57BL/6J mice red line represents DSPP-/- mice. C57BL/6J mice had higher BMD at 1 month of age. At 3 months of age, C57BL/6J had higher BMD, and at 6 months, there was no significant difference between the two groups.

sample architectures was still noticeable but milder. The alveolar bone in the DSPP-/- mice was detected at a lower level than observed in C57BL/6J mice. At 6 months of age, mild differences can still be noticed between the DSPP-/- and C57BL/6 alveolar bone. DSPP-/- mice had a more porous alveolar bone structure than C57BL/6J mice. (figure3.8)

3.3.2 Condyle

At 1 month of age, severe demineralization can be noticed in the DSPP-/- condyle head. The DSPP-/- 1-month-old condyle head appears rougher and more porous than the smooth condyle head in the C57BL/6J image. At 3 months of age, milder demineralization can be noticed in the DSPPP-/- image. The 3 months of age DSPP-/- condyle appears rougher than the C57BL/6J. At 6 months of age, no significant difference could be noticed between the C57BL/6J and DSPP-/- condyles. (figure 3.9)

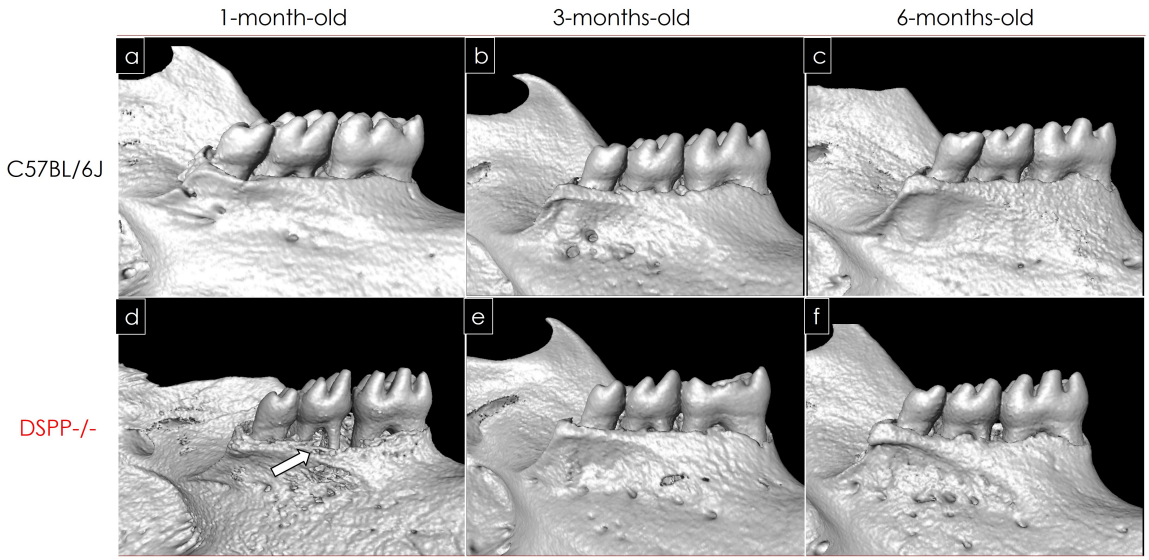

Figure 3.8: Micro-CT images of 1, 3, and 6-months old mice alveolar bone. Figures 3.8 (a-c) represent C57BL/6J mice, and figures 3.8 (d-f) represent DSPP-/- mice. Figures 3.8 (a-c) show smooth bone surface structure. Severe demineralization is present in figure 3.8 (d), and figure 3.8 (e-f) shows porosities in the alveolar bone.

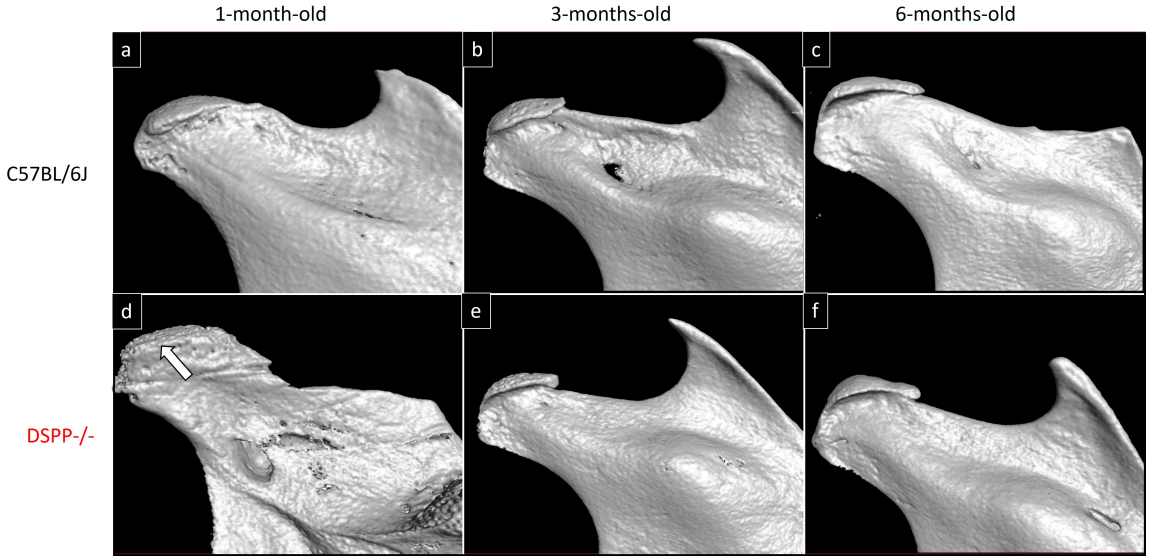

Figure 3.9: Micro-CT images of 1, 3, and 6-months old mice condyle. Figures 3.9 (a-c) represent C57BL/6J mice, and figures 3.9 (d-f) represent DSPP-/- mice. Smooth condyle surface can be noticed in figures 3.9 (a-c) and figure 3.9 (f). Severe demineralization can be noticed in figure 3.9 (d). Porosities are also noticed in figure 3.9 (e).

3.3.3 Long Bone

Long bone images did not show significant differences in bone surfaces between the C57BL/6J and DSPPP-/- in any age group. (figures 3.10)

Figure 3.10: Micro-CT images of 1, 3 6-months old mice long bone. Figures 3.10 (a-c) represent C57BL/6J mice, and figures 3.10 (d-f) represent DSPP-/- mice. No clear differences in bone surface structures could be noticed between the DSPP-/- and C57BL/6J images.

3.3.4 Skull

At 1 and 3 months of age, demineralization could be noticed in DSPP-/- skull surfaces. DSPP -/- images showed frontal and parietal bones with significant porosities around the sagittal suture compared to C57BL/6J samples. At 6 months of age, no significant differences could be noticed between the two skull surfaces. (figure 3.11).

3.4 Cell Culture

Alizarin red staining was used to investigate calcium deposits at 0, 7, 14, and 21 days of osteoblast culture from C57BL/6J and DSPP-/- samples. At 0 and 7 days, no calcium deposits were visualized in both C57BL/6J and DSPP-/- cultured cells.

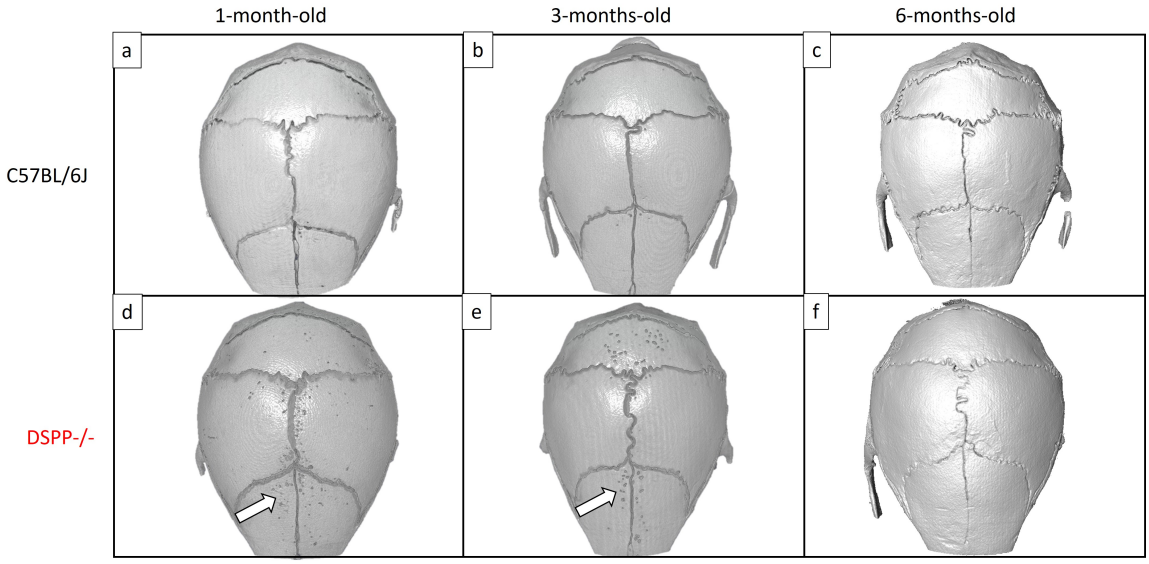

Figure 3.11: Micro-CT images of 1, 3, and 6-months old mice skulls. Figures 3.11 (a-c) represent C57BL/6J mice, and figures 3.11 (d-f) represent DSPP-/- mice. C57BL/6J images in all age groups show smooth skull surface structure [figures 3.11 (a-c)]. DSPP-/- images show porosities on the bone surface structure at 1 and 3 months of age [figures 3.11 (d-e)]. The 6 months old DSPP-/- image shows a smooth bone surface structure [figure 3.11 (f)]

At 14 days, the difference in staining between DSPP-/- and C57BL/6J cultures was detected, with more intense alizarin red staining on C57BL/6J cultured cells. On day 21, the difference in staining between C57BL/6J and DSPP-/- cultures was obvious, with more intense staining observed on C57BL/6J cultured cells. (figure 3.12).

3.5 Hematoxylin and Eosin

3.5.1 Dentin

Differences in dentin and pulp structures were visualized in all three age groups between C57BL/6J and DSPP -/- samples. At 1, 3, and 6 months of age, C57BL/6J showed a well-defined predentin layer with uniform thickness. Normal dentin mineralization with organized dentinal tubules and clearly defined odontoblastic cell layer could also be observed. 1-month-old DSPP -/- showed less organized dentinal tubules and poorly defined predentin layer with unorganized pulpal tissues compared to

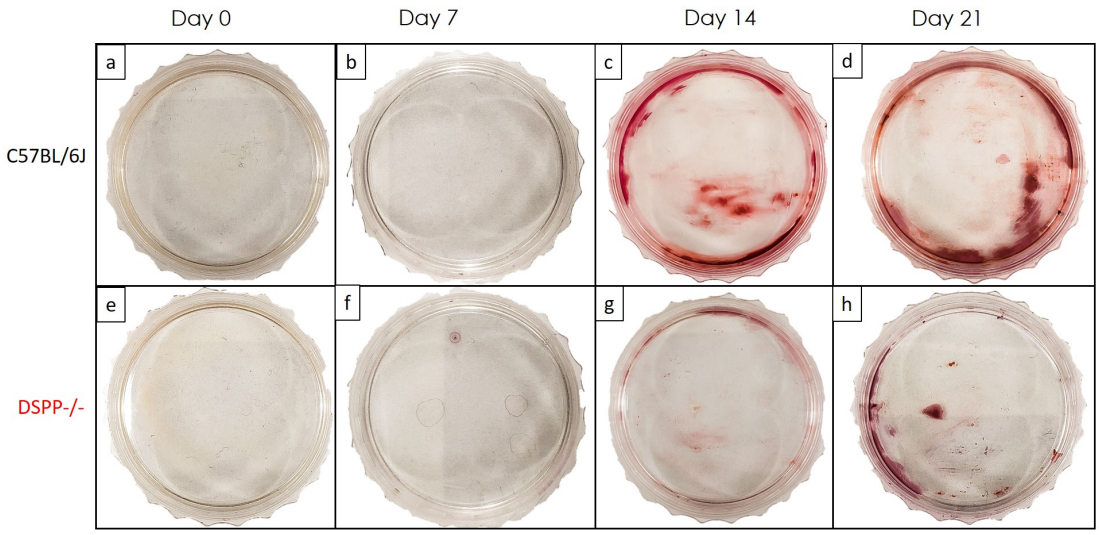

Figure 3.12: Alizarin red staining on osteoblast culture for days 0, 7, 14, and 21. Figures 3.12 (a-d) represent C57BL/6J osteoblasts, and figures 3.12 (e-h) represent DSPP-/- osteoblasts. Figures 3.12 (a-b) and 3.12 (e-f) showed no significant difference in staining. Figures 3.12 (c) and 3.12 (d) showed stronger alizarin red staining compared to figures 3.12 (g) and (h), respectively.

C57BL/6J of the same age group. At 3 months of age, the predentin layer in the DSPP-/- image could not be observed. The dentin of the 3 months old DSPP-/- showed severe demineralization compared to the C57BL/6J of the same age group. Severely disorganized pulpal tissue was observed in the DSPP-/- 3 months-old images. Images from 6 months of age DSPP -/- samples showed poorly defined predentin layers and defective dentin mineralization with areas of interglobular dentin. Disrupted pulpal tissue could also be observed in the 6 months old DSPP-/- image. (figure 3.13).

3.5.2 Periodontium

Differences in alveolar bone and periodontal ligament (PDL) morphology were observed in the three age groups between C57BL/6J and DSPP -/- samples. At 1, 3, and 6 months of age, the C57BL/6J mice presented well-organized PDL fibers and regular thickness of interdental and inter-radicular alveolar bone. DSPP -/- 1-month-

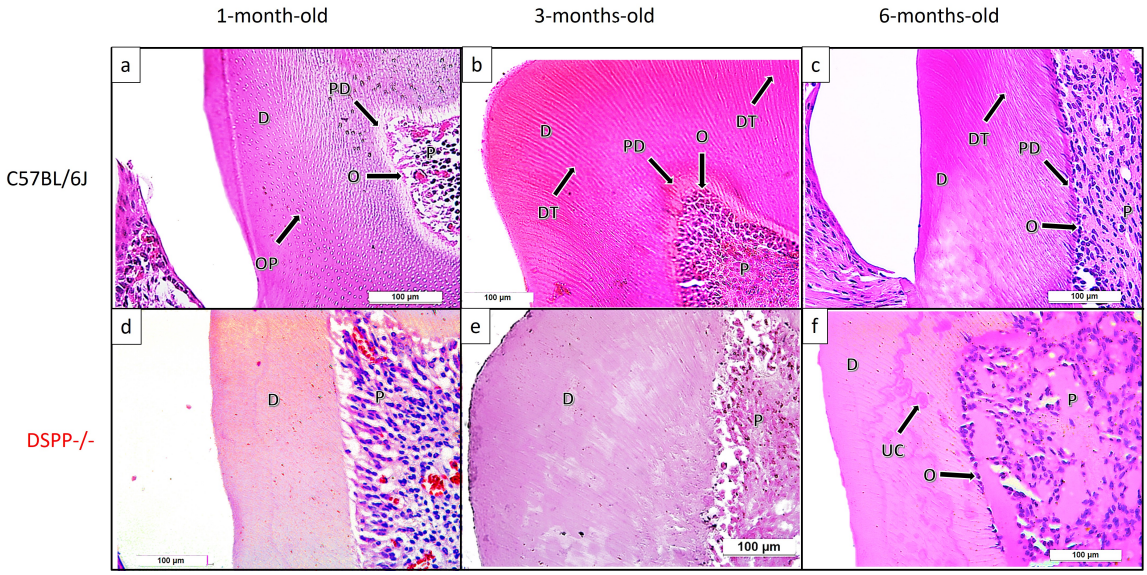

Figure 3.13: H&E staining of 1, 3, and 6-months old mice dentin. Figures 3.13 (a-c) represent C57BL/6J mice, and figures 3.13 (d-f) represent DSPP-/- mice. Figures 3.13 (a-c) show well-defined predentin, dentinal tubules, and osteoblast layer in the pulp. In contrast, no predentin layer could be identified in Figure 3.13 (d-f). D: Dentin. DT: Dentinal Tubules. P: Pulp. PD: Predentin Layer. O: Odontoblast Layer. OP: Odontoblastic processes. UC: Uncoalescent calcospherites.

old images showed less organized PDL fibers and less inter-radicular alveolar bone. Thinner interdental alveolar bone thickness was seen in the 1-month-old DSPP-/- group compared to the C57BL/6J mice of the same age. At 3 and 6 months of age, the interdental and inter-radicular alveolar bone presented less bone within the alveolar bone crest at a lower level in DSPP-/- images compared to C57BL/6J image of the same ages. Less organized PDL fibers and widening of the PDL were also observed in the 3 and 6 months old DSPP-/- image compared to the C57BL/6J images of the same group. (figures 3.14 and 3.15).

3.5.3 Mandibular Condylar Cartilage

The MCC is divided into the following layers: articular layer, prechondroblastic layer, chondroblastic layer, hypertrophic layer, and cartilage-bone interface. It was noticeable at 1 and 3 months of age that the chondroblastic layer was wider in C57BL/6J images compared to the DSPP-/- images. Moderate disorganization of the

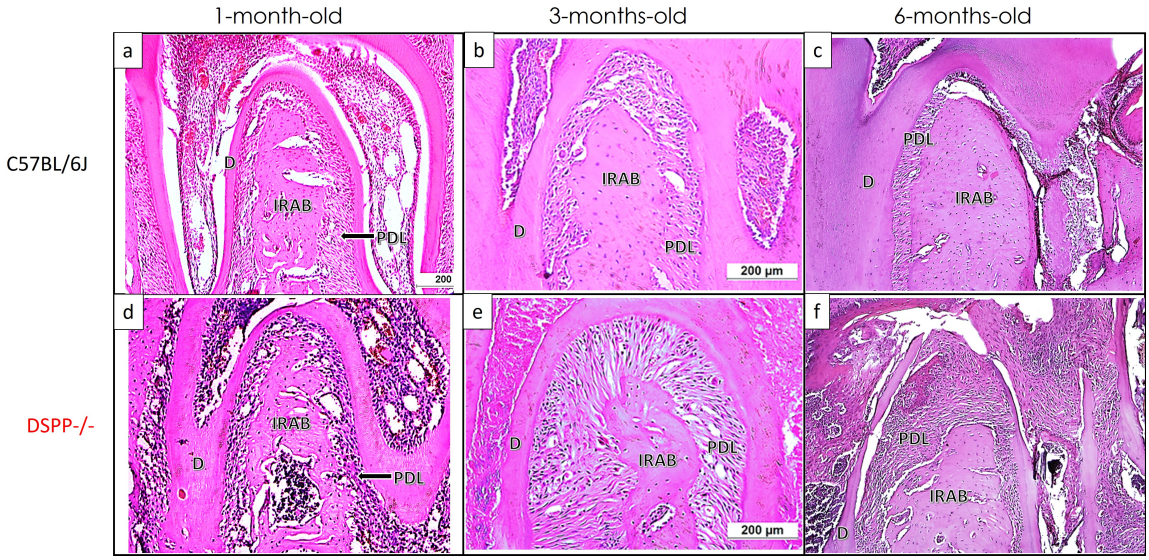

Figure 3.14: H&E staining of 1, 3, and 6-months old mice alveolar bone. Figures 3.14 (a-c) represent C57BL/6J mice, and figures 3.14 (d-f) represent DSPP-/- mice. Figures 3.14 (d-f) show less alveolar bone compared to figures 3.14 (a-c). D: Dentin. IRAB: Inter-radicular alveolar bone. PDL: Periodontal ligament

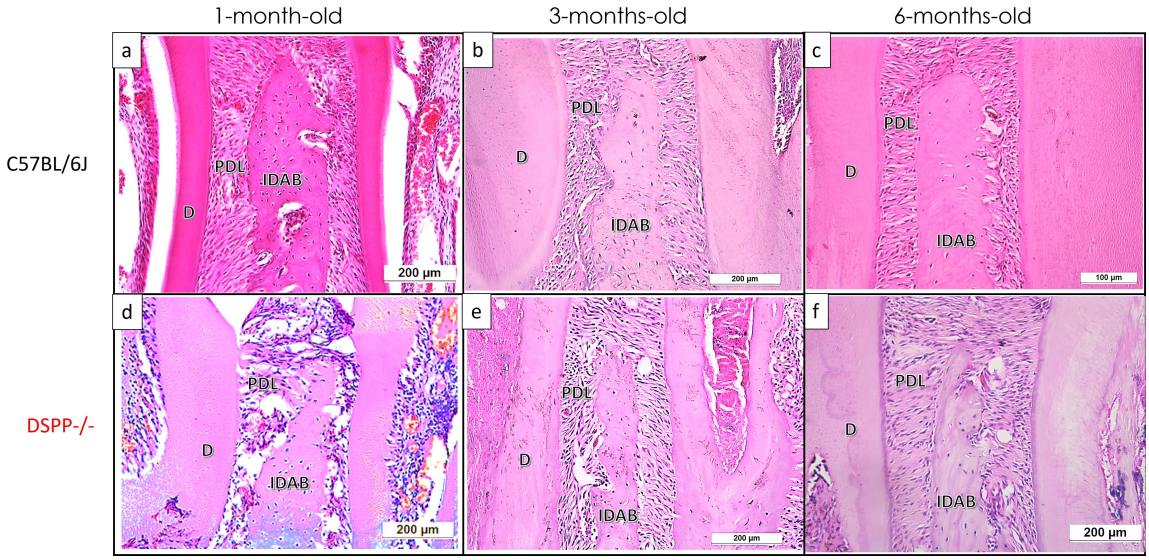

Figure 3.15: H&E staining of 1, 3, and 6-months old mice alveolar bone. Figures 3.15 (a-c) represent C57BL/6J mice, and figures 3.15 (d-f) represent DSPP-/- mice. Figures 3.15 (d-f) show less alveolar bone compared to figures 3.15 (a-c). D: Dentin. IDAB: Interdental alveolar bone. PDL: Periodontal ligament.

chondroblasts was also noticed in 1 and 3 months of age DSPP-/- images In the 6 months old DSPP-/- image, the chondroblastic layer was wider than in the C57BL/6J image. There was no significant difference in all other layers between C57BL/6J and

DSPP-/- in any of the age groups. (figure 3.16).

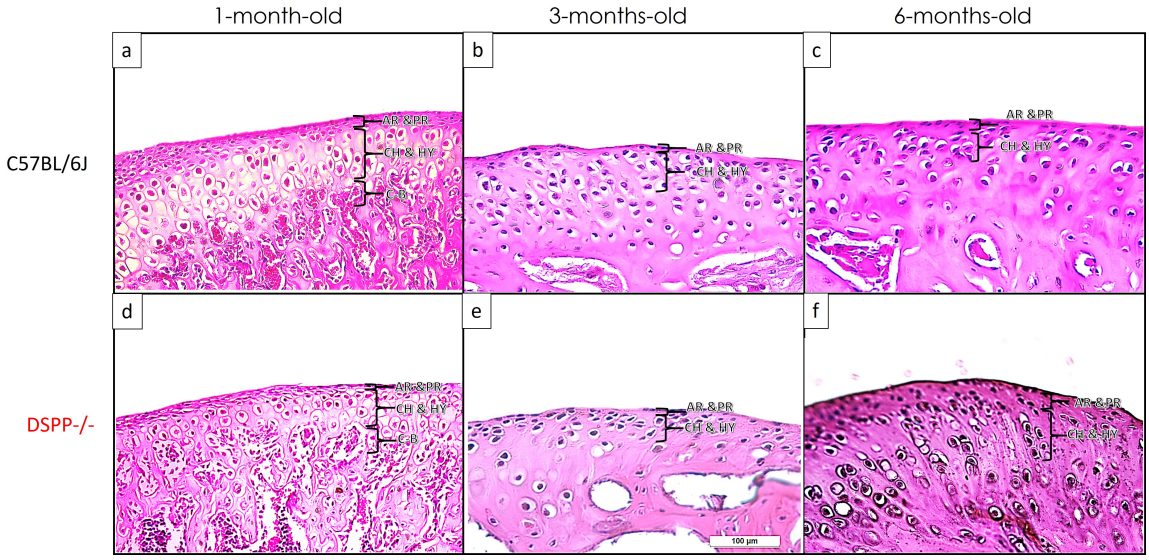

Figure 3.16: H&E staining of 1, 3, and 6-months old mice mandibular condylar cartilage. Figures 3.16 (a-c) represent C57BL/6J mice, and figures d-f represent DSPP-/- mice. Figures 3.16 (a-b) show wider chondroblastic and hypertrophic layers compared to figures 3.16 (d-e). Figure 3.16 (f) shows wider chondroblastic and hypertrophic layers compared to figure 3.16 (c). AR: Articular. PR: Prechondroblastic. CH: Chondroblastic. HY: Hypertrophic. C-B: Collagen-bone.

3.5.4 Long Bones

Differences were noticed in the articular cartilage region of the distal femoral condyle at 1 month of age between C57Bl/6J and DSPP-/- images. The hypertrophic and chondroblastic layers of the C57BL/6J samples were wider than those in the DSPP-/- image of the same age. Clear differences could not be observed between C57BL/6J and DSPP-/- images from 3 and 6 months of age groups. (figure3.17)

3.5.5 Skulls

H&E stained images of skulls showed noticeable deposition lines in C57BL/6J images in 1, 3, and 6 months of age. DSPP-/- images did not show deposition lines in any of the three age groups. Deposition lines indicate mineralization zones. (figure3.18)

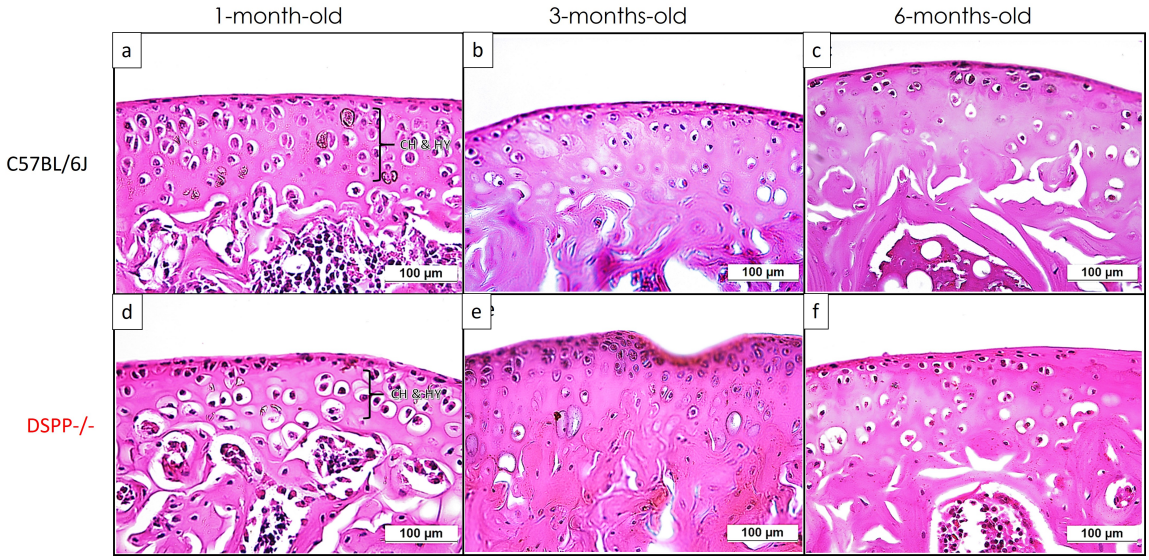

Figure 3.17: H&E staining of 1, 3, and 6-months old mice long bone articular cartilage. Figures 3.17 (a-c) represent C57BL/6J mice, and figures 3.17 (d-f) represent DSPP-/- mice. Figure 3.17 (a) shows wider chondroblastic and hypertrophic layers compared to figure 3.17 (d). Figures 3.20(d) and 3.20(f) also show disorganized chondroblasts. CH: Chondroblastic. HY: Hypertrophic.

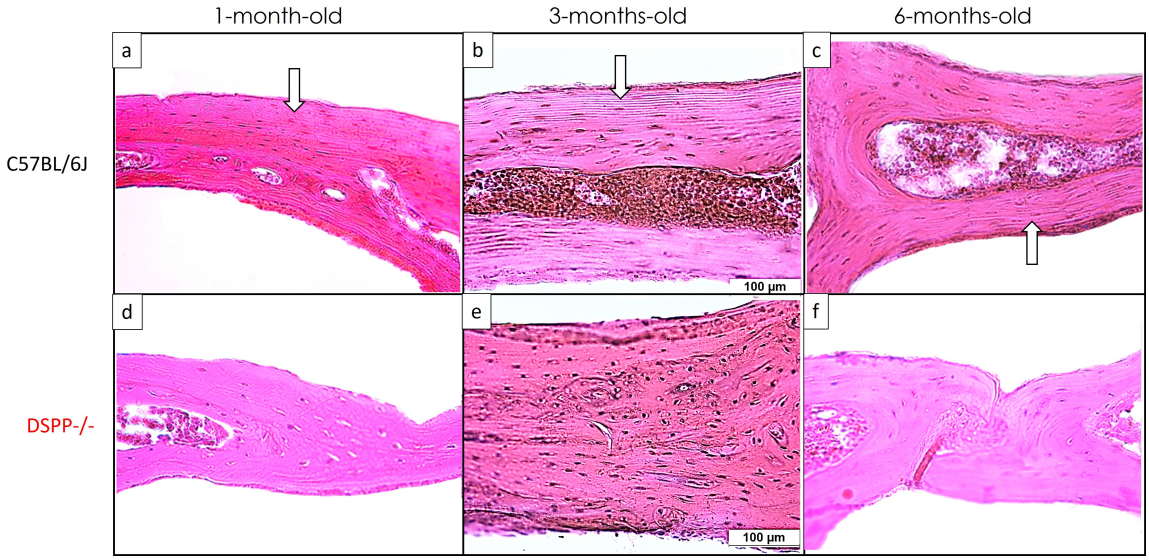

Figure 3.18: H&E staining of 1, 3, and 6-months old mice skull. Figures 3.18 (a-c) represent C57BL/6J mice, and figures 3.18 (d-f) represent DSPP-/- mice. Mineral deposition lines can be seen in figures 3.18 (a-c). In contrast, no mineral deposition lines can be seen in figures 3.18 (d-f).

3.6 Immunohistochemistry Staining

Clear differences in immunohistochemistry staining of DSP intensity could be noticed between C57BL/6L samples and DSPP-/-. Anti-DSP staining was remarkably noticed in C57BL/6L samples at all age groups, contrary to all DSPP -/- samples. In dentin, anti-DSP staining showed strong intensity in the predentin region and around dentinal tubules in C57BL/6J images in all age groups. Anti-DSP staining in the DSPP-/- group showed negative signals. (figure3.19)

In MCC, anti-DSP staining showed strong intensity in the prechondroblastic, chondroblastic, and hypertrophic layers of the C57BL/6J images at 1 and 3 months of age. At 6 months of age, the C57BL/6J image showed a moderate intensity of anti-DSP staining. DSPP-/- images showed negative signals in all age groups. (figure3.20)

In alveolar bone, anti-DSP staining was present in C57BL/6J images at 1, 3, and 6 months of age. In DSPP-/-, the staining signal for anti-DSP was negative in all age groups. (figure3.21)

In long bone articular cartilage, anti-DSP staining was present at a mild intensity in C57BL/6J images in 1 and 3 months of age and at a stronger intensity at 6 months of age. In DSPP-/-, the staining signal for anti-DSP was negative in all age groups. (figure3.22)

In skulls, anti-DSP staining was detected in C57BL/6J images at 1, 3, and 6 months of age, contrary to the DSPP-/- images of the same ages. (figure3.23)

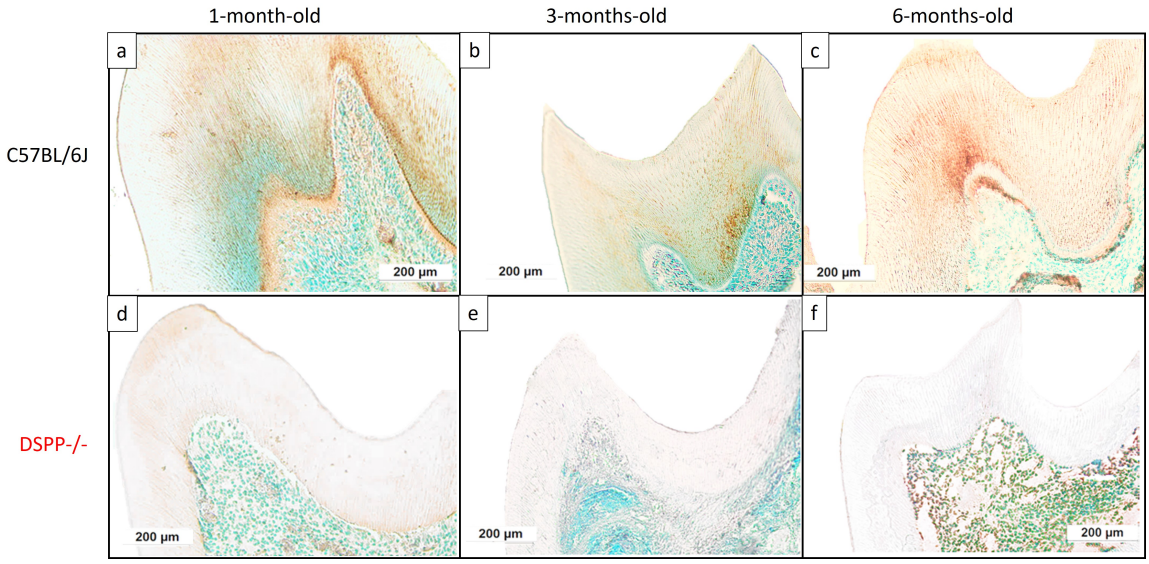

Figure 3.19: IHC staining images of Anti-DSP signal in 1, 3, and 6-months old mice dentin. Figures 3.19 (a-c) represent C57BL/6J mice, and figures (d-f) represent DSPP-/- mice. A strong anti-DSP signal was detected around predentin and dentinal tubules regions in figures 3.19 (a-c).

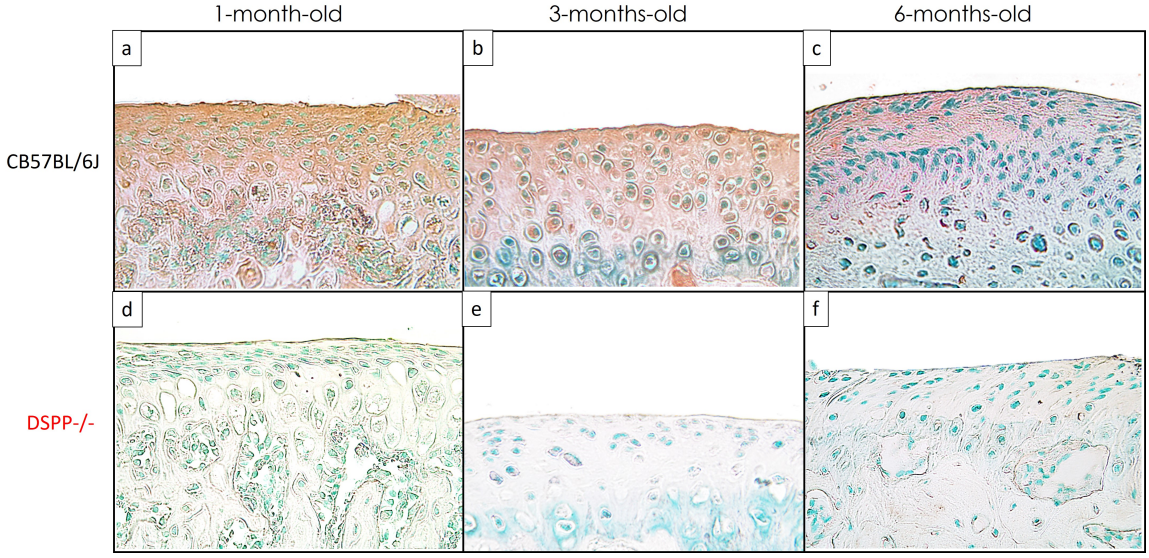

Figure 3.20: IHC staining of Anti-DSP signal in 1, 3, and 6-months old mice mandibular condylar cartilage. Figures 3.20 (a-c) represent C57BL/6J mice, and figures 3.20 (d-f) represent DSPP-/- mice. A strong anti-DSP signal was detected in the prechondroblastic and chondroblastic layers in figure 3.20 (a-c).

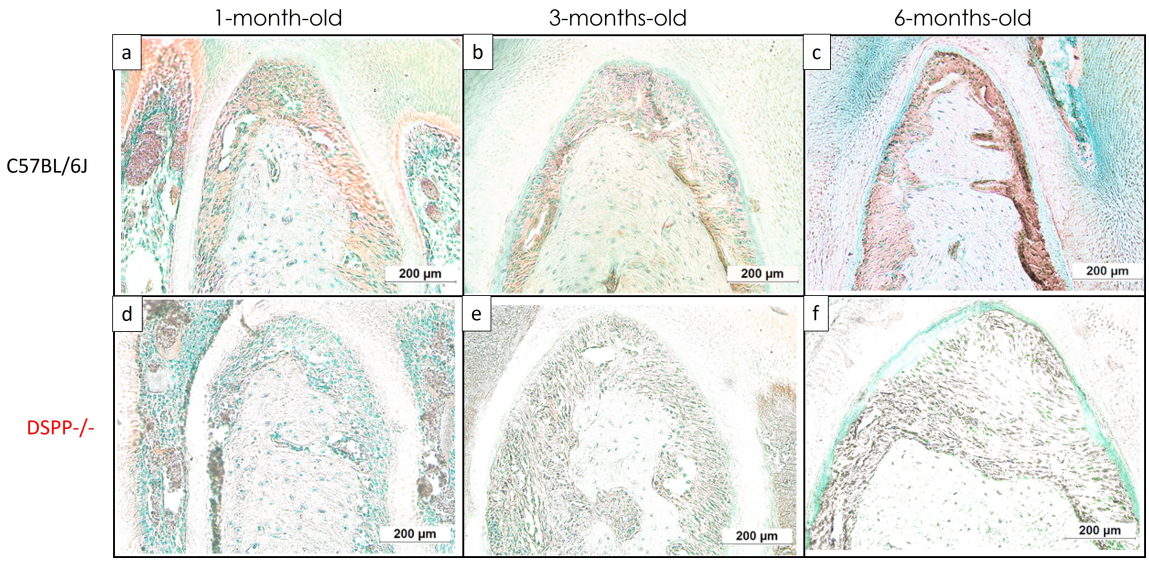

Figure 3.21: IHC staining of Anti-DSP signal in 1, 3 and 6-months old mice alveolar bone. Figures 3.21 (a-c) represent C57BL/6J mice, and figures 3.21 (d-f) represent DSPP-/- mice. An Anti-DSP signal was detected in figures 3.21 (a-c).

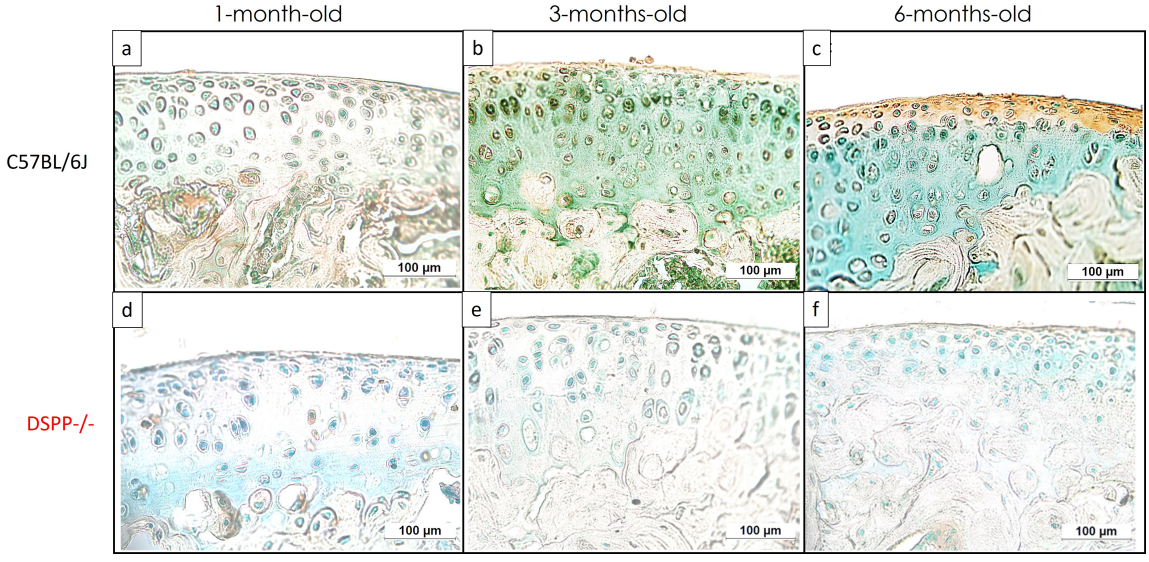

Figure 3.22: IHC staining of Anti-DSP signal in 1, 3, and 6-months old mice long bone articular cartilage. Figures 3.22 (a-c) represent C57BL/6J mice, and figures 3.22 (d-f) represent DSPP-/- mice. An Anti-DSP signal was detected in figures 3.22 (a-c), with stronger intensity on the articular surface.

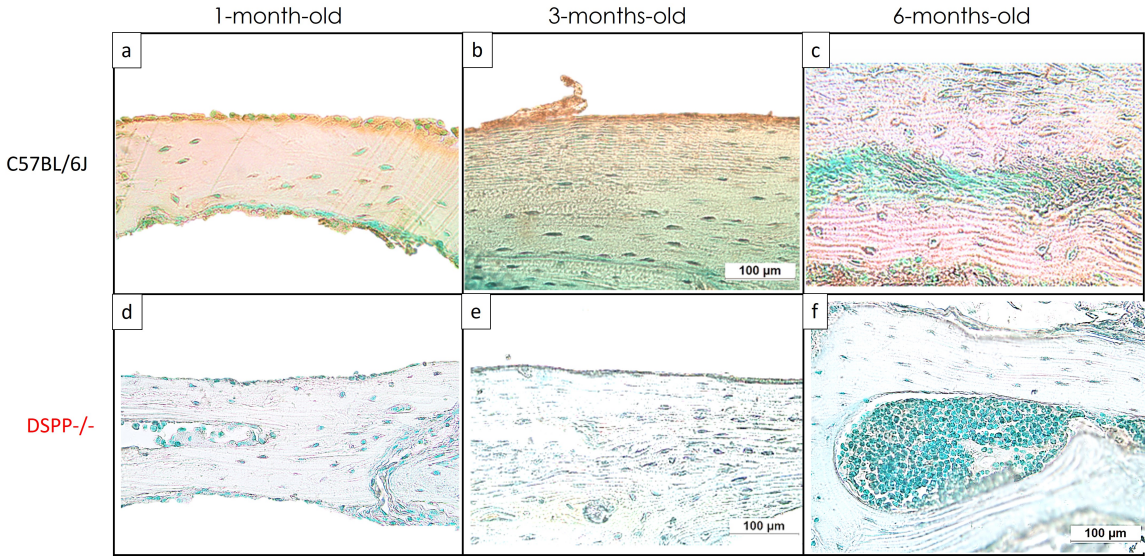

Figure 3.23: : IHC staining of Anti-DSP signal in 1, 3, and 6-months old mice skull. Figures 3.23 (a-c) represent C57BL/6J mice, and figures 3.23 (d-f) represent DSPP-/- mice. An Anti-DSP signal was detected in figures 3.23 (a-c), with stronger intensity on the surface region of the skull.

Chapter 4

Discussion

Bone and dentin are similar in composition and mechanism of mineralization. They originate from osteoblasts and odontoblasts, respectively. Osteoblasts and odontoblasts secrete an unmineralized matrix rich in type I collagen called osteoid and predentin, respectively. These unmineralized matrixes lie between their originating cells and the mineralization front. In the mineralization front, HA crystals are deposited to form bone and dentin. Mineralization of osteoid and predentin involves an interplay between type I collagen and different NCPs.[86] DSPP is known to be extremely important in controlling the mineralization of predentin.[34]–[36] With the recent discovery of DSPP expression in several non-dental tissues [54], the importance of investigating its role in different tissues came to light.

Previous studies have investigated the role of DSPP in dentinogenesis and long bone mineralization. [34]–[36], [56], [83] However, this study, for the first time, investigated the impacts of DSPP deletion in the mandibular condylar cartilage and craniofacial complex of mice at 1, 3, and 6 months of age using a variety of methods.

Congenital anomalies affect 2 to 3% of babies born worldwide, and craniofacial defects are often associated with these anomalies. [87] Ultimately, the findings of the present study could be used to identify target proteins with rescue potential to craniofacial defects.

4.1 Molars

Radiographic images of Faxitron Ultra Focus DXA are the result of x-ray beams passing through tissues and being absorbed. [88] There is a positive correlation between tissue mineralization and x-ray absorption. Structures that absorb higher amounts of x-ray appear as opaque regions in the radiographic image. Those are named radiopaque structures. The most radiopaque structure in teeth is the enamel, as it is 99% inorganic.[89] Structures where the x-rays simply pass through, with low absorption, are named radiolucent. The tooth pulp, for example, is an unmineralized structure, and it appears as a radiolucent region in a radiographic image.[90] Therefore, radiographic images are a great tool to identify mineralization defects.

Radiographic results from this study showed clear differences between C57BL/6J and DSPP -/- mice molars at all investigated ages. It is known from the previous literature that the deletion of DSPP protein causes severe defects in dentin mineralization.[84][81] Thus, it was expected that the lack of mineralization would result in more radiolucent molars in DSPP-/- images. In fact, this has been shown previously.[66]

In C57BL/6J images, all dental structures could be identified. As expected from their mineral composition, enamel showed the most radiopaque structure. Dentin, which is 70% inorganic, could be identified as a radiopaque structure, and pulp appeared as a radiolucent structure.

All age groups of DSPP-/- molar images showed a much thinner enamel layer and a barely visible dentin layer. Such results suggest severe demineralization of the dental structure. Extensive radiolucent regions were noticed in DSPP-/-molars, suggesting demineralization of dentin. This demineralization took place due to the defective formation of dentin and further destruction from cariogenic activity. This cariogenic

destruction is expected in teeth with reduced mineral content. [91]

DXA investigation of dentin and enamel regions was used as a control for DXA analysis, as it is known that the absence of DSPP protein severely affects the formation of dentin. DXA results showed significantly lower BMD in all age groups in DSPP-/- samples compared to C57BL/6J, confirming the results seen in other radiographs.

H&E staining of molars showed differences in all age groups between DSPP-/- and C57BL/6J samples. At 1 and 3 months of age, a normal predentin layer in C57BL/6J was observed with normal dentin formation and mineralization. As well as organized pupal tissues with clearly defined odontoblast layer. In contrast, in DSPP-/- mice of the same age groups, a predentin-dentin interface is difficult to be identified, and the predentin layer was widened. Also, no well-defined layer of odontoblasts was detected at the pulp boundaries in the DSPP-/- images. The predentin layer anomalies suggest that dentin mineralization might be occurring at a slower rate in DSPP-/-. Inflammation was observed in the DSPP-/- pulp in all age groups, and it may have affected the adjacent odontoblasts with resulting poorly defined layer of odontoblasts.

DSPP is known to have an active role in the mineralization front of the predentin. One of its cleaved fragments, DPP, binds to collagen to promote the formation of HA crystals.[92], [93] Therefore, defective formation of HA crystals and defective mineralization of predentin into dentin might be related to the absence of DSPP protein.

At 6 months of age, differences in the maturation of the dentin are clear. Uncoalescent calcospherites, or interglobular dentin, are seen in DSPP-/- samples. Interglobular dentin is the result of the inability of mineralization centers in the dentin to merge, therefore, leaving regions of hypomineralized dentin matrix in the dentin

structure. [94] Collagen deposition was also observed in the pulp of 6 months old DSPP-/- mice, and may have occurred as a reaction to chronic inflammation.

The present study analyzed anti-DSP signal in C57BL/6J compared to DSPP-/- samples at 1, 3, and 6 months of age. C57BL/6J images showed anti-DSP signals that varied with age and type of tissue.

Molar results showed that the anti-DSP signal is stronger in the predentin and dentinal tubules regions. This expression pattern is following previous literature that described regions where DSPP protein acts during dentin mineralization. [92], [93]

4.2 Alveolar bone

The alveolar bone is a mineralized structure 60% composed of inorganic material.[4] Therefore, it is expected to be identified as a radiopaque structure with similar opacity to dentin in radiographic images. C57BL/6J images showed clearly defined alveolar bone as radiopaque structures at 1, 3, and 6 months of age. However, in DSPP-/- images from all investigated ages, radiolucent regions could be identified around the roots of the molars, suggesting bone demineralization.

It is important to note that such demineralization of alveolar bone could be happening as a primary consequence of the absence of DSPP in the mineralization process or as a secondary reaction to cariogenic activity that caused an inflammation of the pulp and subsequent alveolar bone inflammatory destruction. In figure 3.1(d), it could be observed that radiolucency of the alveolar bone was present even though the molar did not show evidence of cariogenic destruction. Therefore, demineralization of the alveolar bone could be attributed to the absence of DSPP protein [82]

Three-dimensional reconstructions of hemi-mandibles yielded images of alveolar bone surface from DSPP-/- and C57BL/6J samples. At 1 month of age, DSPP -/-

samples had a rough and porous alveolar bone exposing root furcation compared to C57BL/6J samples. This might suggest severe demineralization in DSPP-/- at this age. At 3 and 6 months of age, differences in alveolar bone were less significant than in 1 month of age. This suggests that the absence of DSPP protein has a greater impact on the alveolar bone at the early stages of development..

All age groups show differences in periodontium anatomy between DSPP-/- and C57BL/6J. At 1, 3, and 6 months of age, less alveolar bone was observed in DSPP-/- samples compared to C57BL/6J. The PDL fibers are less organized both in the interdental and interalveolar regions in DSPP-/- images compared to C57BL/6J in all ages, suggesting demineralization in DSPP-/- samples.

DSPP is highly expressed in the alveolar bone. [51] Alveolar bone defects in the absence of DSPP are likely related to the loss of function of the DSPP protein rather than secondary to pulp inflammation (pulpitis). H&E staining results showed that alveolar bone defects are present from early ages before pulpitis develops. However, pulpitis that progressed to inflammation in the alveolar bone region might have caused further destruction.

Previous studies have suggested that DSP is secreted by osteoblasts, cementoblasts, and fibroblasts in the alveolar bone and PDL. [51] In our study, anti-DSP signal could be identified in C57BL/6J alveolar bone and PDL at 1, 3 and 6 months of age. Our results are in accordance with published literature.

4.3 Mandibular condyle and MCC

The mandibular condyle is a mineralized structure with a 60% inorganic composition.[4] The articular surface and the condylar process are regions where bone tissue is the most condensed. Therefore, those are the most radiopaque structures of the

condyle. To our knowledge, the impacts of DSPP deletion during development in these tissues have not been previously studied.

Radiographic images showed clearly defined radiopaque regions in the condyle articular surface and the condylar process of C57BL/6J samples at all investigated ages. DSPP-/- images showed different results from C57BL/6J in all investigated ages. Regions of higher radiopacity could be seen at the condyle articular surface region in DSPP -/- images at 1 month of age, showing a region of advanced mineralization. This suggests that DSPP could have a regulatory function in the mineralization of the articular surface at an early age.

At 3 and 6 months of age, results showed a poorly defined and less radiopaque condylar process in DSPP-/- images compared to C57BL/6J images of the same age groups. This finding suggests a less mineralized condylar process in DSPP-/- compared to C57BL/6J condyles. This could result in a weaker condyle structure more prone to fractures in DSPP -/- mice. Expression of DSPP in the mandibular condyle has been evidenced before. However, this is the first study to analyze the impacts of DSPP deletion on the condyle. These results suggest that DSPP is not only expressed but also plays an active role in the mineralization process of the mandibular condyle.

It is known that DSPP is expressed in the MCC but no reports of its role in the MCC development have been published to our knowledge.[23], [54] MCC had higher BMD in DSPP -/- samples at 1-month demineralization of age compared to C57BL/6J. However, at 3 months of age, C57BL/6J samples had higher BMD compared to DSPP-/-. At 6 months of age, no significant difference was present between the groups. This suggests that DSPP might have a role in regulating the mineralization process in the MCC region at the early stages of development.

Three-dimensional reconstructions of hemi-mandibles showed severe demineralization in DSPP-/- samples at 1 month of age. DSPP-/- condyle appeared rougher and more porous compared to the C57BL/6J condyle. At 3 months of age, DSPP-/- condyle showed demineralization at a milder level than 1 month of age. At 6 months, both groups showed a similar condyle structure. This suggests that DSPP absence affects early stages of development more severely than advanced stages of development in condyles.

It is important to compare the results between the methods, although the DSPP -/- MCC had higher BMD at 1 month of age and appeared more radiopaque in radiographic images, the micro-CT image shows that the surface of the bone formed was of poor quality. This suggests that in early ages DSPP acts as a regulator of mineralization in the MCC.

H&E staining images of the mandibular condylar cartilage show thinner prechondroblastic, chondroblastic, and hypertrophic layers in DSPP-/- samples at 1 and 3 months of age compared to C57BL/6J samples. However, at 6 months of age, these layers appeared wider in the DSPP-/- image. Previous literature has concluded that the loss of DSPP impacts the development of different layers of the MCC.[95] DSPP has also been found to be mainly expressed in the articular and prechondroblastic layers in neonatal mice, and the loss of function of DSPP affects these layers at the early stage of development.[23] The impacts of DSPP loss of function in the MCC layers might be related to mineralization defects observed in micro-CT results.

Anti-DSP signal was detected with strong intensity in the MCC articular and prechondroblastic layers at 1 and 3 months of age in C57BL/6J images. This is following previous literature which suggested that DSPP is important for the development of those layers at an early stage of development.[23]

4.4 Long bone

The long bone is composed of cortical and trabecular bone. The cortical bone is more mineralized and, therefore, more radiopaque. The trabecular bone contains intertrabecular spaces that are less mineralized and, therefore, less opaque in radiographic images. The long bone is divided into three regions, diaphysis, growth plate, and epiphysis. During development, new bone is formed from the growth plate. The growth plate is non-mineralized cartilage, and therefore, a radiolucent structure in radiographic images. After development is finished, the remainder of the growth plate can be seen radiographically as a line between the diaphysis and epiphysis, known as the epiphyseal line.[96]

Radiographic images of long bones showed mild differences between DSPP -/- and C57BL/6J samples at 1 month of age. The DSPP-/- image showed an enlarged growth plate compared to the one in the C57BL/6J image. The growth plate is most important at an early age. After the growth plate finishes development, it fuses with the bone to become an epiphyseal line. An enlarged growth plate indicates that mineralization is slower in DSPP-/- mice compared to C57BL/6J mice. Results from 3 and 6 months of age mice did not show clear differences between the radiographs of C57BL/6L and DSPP-/- mice.

Expression of DSPP in the long bone is weaker than in the MCC.[54] In the current study, BMD results in long bones were significantly higher in C57BL/6J mice compared to DSPP-/- mice at 1 and 3 months of age. No significant difference was observed at 6 months of age between the groups. This suggests that DSPP is active in the mineralization process of the long bone.

Three-dimensional reconstruction of long bone did not show clear differences in the bone surface between DSPP-/- and C57Bl/6J samples in all age groups.

H&E staining images of long bone articular cartilage showed wider chondroblastic and hypertrophic layers in the C57BL/6J compared to the DSPP-/- image at 1 month of age. No differences were noticed when comparing DSPP-/- to C57BL/6J images at 3 and 6 months of age. DSPP is expressed at a lower level in the long bone when compared to MCC. [95] However, both MCC and long bone articular cartilage show similar defects in their layers in the absence of DSPP at 1 month of age. Therefore, our results suggest that the role of DSPP in the articular cartilage of the long bone might be similar to the role of DSPP in the MCC at an early stage of development.

DSPP is known to be expressed at a lower level in the long bone than at the MCC and dentin.[54] In our study, anti-DSP signal was detected in the articular cartilage of C57BL/6J mice at 1, 3 and 6 months of age. Anti-DSP signal detected in the articular cartilage was weaker than the anti-DSP signal observed in the MCC and dentin images.

4.5 Skull

Radiographic images of skulls are limited by the superposition of structures. This is caused by trying to represent a three-dimensional object in a two-dimensional plane. Due to the superposition of structures, no difference could be noticed in radiographic images of skulls between C57BL/6J and DSPP-/- samples at 1, 3 or 6 months of age. However, a past study has determined that radiographic images of DSPP-/- calvaria are less radiopaque than C57BL/6J ones at 1, 2, and 3 months of age.[81] Suggesting that the abscence of DSPP protein is negatively impacting mineralization of the calvarium bones. In our study, skull surfaces were further analyzed with micro-CT.

Micro-CT images of calvarium surfaces showed clear differences at 1 and 3 months of age. Rougher and more porous calvarium surfaces were observed in DSPP-/- samples compared to C57BL/6J. At 6 months of age, DSPP-/- and C57BL/6J samples did

not show clear differences. Suggesting that DSPP's role in the mineralization process of the calvaria is active during the early stages of development.

At 6 months of age, differences could not be seen in MCC, alveolar bone, and calvaria between C57BL/6J and DSPP-/- samples. Both in BMD results and micro-CT images. This suggests that other NCPs might be compensating the absence of DSPP.

Genetic compensation is defined as changes in protein levels aimed at compensating for the loss of function of another gene. Differences between samples were the most noticeable at 1 month of age, while at 6 months of age, samples looked similar. There is limited literature on the mechanisms of compensation. It is possible that upregulation of other SIBLING proteins, such as the ones mentioned previously, might be occurring to compensate for the DSPP absence.[97]

In H&E staining images of the skull, incremental apposition lines can be seen in C57BL/6J samples in all investigated ages. In contrast, no incremental apposition lines were noticed in DSPP-/- samples at any age. Incremental apposition lines have been described as a sign of bone remodeling in previous literature.[98] Micro-CT results also showed that DSPP-/- calvaria is more porous than C57BL/6J calvaria at 1 and 3 months of age. Our results suggest that bone formation and remodeling occur with a better organization in C57BL/6J compared to DSPP-/- skulls.

Cell culture protocol was done according to Chen et al.[81] Cells were extracted from the calvaria of one C57BL/6J and one DSPP-/- mouse. At days 0 and 7, no difference in Alizarin red staining intensity was observed between C57BL/6J and DSPP-/- calvarial cultures. Calvarial osteoblast culture showed stronger calcium and phosphate deposits staining in C57BL/6J cultures compared to DSPP-/- cultures at 14 and 21 days. These results suggest that differentiation of mesenchymal stem

cells into osteoblasts and function of osteoblasts might be negatively impacted in the absence of the DSPP protein. The limitation of this observation was the sample size of one mouse per group.

To our knowledge, this was the first investigation of DSPP expression in the skull calvaria. Our results showed stronger anti-DSP signal at 1 and 3 months than at 6 months of age in the C57BL/6J calvaria. This, alongside micro-CT results of the calvaria surface, suggest that DSPP might be important for normal mineralization of the calvaria during early stages of development.

Chapter 5

Conclusions, Recommendations, & Future Work

5.1 Conclusions

Findings suggest that DSPP knockout affects early ages more severely than mature ones. Our results thoroughly investigated the changes in the histology and anatomy between the C57BL/6J and DSPP-/- mice.

We came to conclude that DSPP is an essential protein for the normal mineralization of craniofacial tissues. It was showed that DSPP absence caused defects in the mineralization of skulls, MCC, and alveolar bones at the early stages of development. However, a potential genetic compensation mechanism might be able to play a role in partially recovering these defects.

5.2 Future Work

Future work should focus on understanding the mechanisms of genetic compensation. Further investigation of which proteins are responsible for this compensation would yield a better understanding of the pathways of mineralization in the body. Identifying these pathways would be essential in contributing to a cure for craniofacial defects associated with genetic anomalies.

Bibliography

[1] B. K. Hall (2005). Bones and Cartilage. Developmental and Evolutionary Skeletal Biology. Chapter 1: Types of Skeletal Tissues; Pages 3-12.

[2] M. Goldberg, A. B Kulkarni, M. Young, A. Boskey (2011). Dentin structure, composition, and mineralization. Frontiers in Bioscience; 13(1), 711–735.

[3] J. M. Mbuyi-Muamba, J Dequeker, and G Gevers (1989). Collagen and Non-Collagenous Proteins in Different Mineralization Stages of Human Femur. Cells Tissues Organs; 134(4), 265–268.

[4] A. L. Boskey (2013). Bone composition: relationship to bone fragility and antiosteoporotic drug effects. BoneKEy Reports; 2(1), 447.

[5] M. L. Bouxsein and E. Seeman (2009). Quantifying the material and structural determinants of bone strength. Best Practice & Research Clinical Rheumatology. 23(6); 741-753.

[6] M. E. Ruppel, L. M. Miller, and D. B. Burr (2008). The effect of the microscopic and nanoscale structure on bone fragility. Osteoporosis International; 19, 1251–1265

[7] L. V. Belousov (2011). Scott F. Gilbert Developmental Biology, Sinauer Associates, Inc., Sunderland, MA Ninth Edition. Russian Journal of Developmental Biology; 42(5), 349.

[8] H. E. Schroeder and H. E. Schroeder (1986). Development, Structure, and Function of Periodontal Tissues. The Periodontium; 23-323.

[9] J. G. Betts, K. A. Young, J. A. Wise, E. Johnson, B. Poe, D. H. Kruse, O. Korol, J. E. Johnson, M. Womble, and P. DeSaix (2013). Anatomy and Physiology. OpenStax.

[10] E. F. Chan, R. Harjanto, H. Asahara, N. Inoue, K. Masuda, W. D. Bugbee, G. S. Firestein, H. S. Hosalkar, M. K. Lotz, and R. L. Sah (2012) Structural and functional maturation of distal femoral cartilage and bone during postnatal development and growth in humans and mice. Orthopedic Clinics of North America; 43(2), 173-185.

[11] A. J. Hayes, S. MacPherson, H. Morrison, G. Dowthwaite, and C. W. Archer (2001). The development of articular cartilage: Evidence for an appositional growth mechanism. Anatomy and Embryology; 204(1), 469–479.

[12] E. B. Hunziker, E. Kapfinger, and J. Geiss (2007). The structural architecture of adult mammalian articular cartilage evolves by a synchronized process of tissue resorption and neoformation during postnatal development.

Osteoarthritis and Cartilage; 15(4), 403–413.

[13] E. Matalova, V. Lungova, and P. Sharpe (2015). Development of Tooth and Associated Structures. Stem Cell Biology and Tissue Engineering in Dental Sciences; 335-346.

[14] M. Hovorakova, H. Lesot, M. Peterka, and R. Peterkova (2018). Early development of the human dentition revisited. Journal of Anatomy; 233(2), 135-145.

[15] A. H. Jheon, K. Seidel, B. Biehs, and O. D. Klein (2013). From molecules to mastication: The development and evolution of teeth. Wiley Interdisciplinary Reviews: Developmental Biology; 2(2), 165-182.

[16] P. Jain and M. Rathee (2020). Embryology, Tongue [Internet].

[17] T. Yu, A. A. Volponi, R. Babb, Z. An, and P. T. Sharpe (2015). Stem Cells in Tooth Development, Growth, Repair, and Regeneration. Current Topics in Developmental Biology; 115, 187-212.

[18] R.D. Knight, T.F. Schilling (2006). Cranial Neural Crest and Development of the Head Skeleton. In: Saint-Jeannet JP. (eds) Neural Crest Induction and Differentiation. Advances in Experimental Medicine and Biology; 589, 120-133.

[19] A. Linde and M. Goldberg (1993). Dentinogenesis. Critical Reviews in Oral Biology Medicine; 4(5), 679–728.

[20] V Raina (1972). Normal osteoid tissue. Journal of Clinical Pathology; 25(3), 229–232.

[21] K. A. Staines, V. E. MacRae, and C. Farquharson (2012). The importance of the SIBLING family of proteins on skeletal mineralisation and bone remodelling. Journal of Endocrinology; 214(3), 241–255.

[22] B. Huang, Y. Sun, I. Maciejewska, D. Qin, T. Peng, B. McIntyre, J. Wygant, W. T. Butler, and C. Qin (2008). Distribution of SIBLING proteins in the organic and inorganic phases of rat dentin and bone. European Journal of Oral Sciences; 116(2), 104–112.

[23] Y Sun, V Gandhi, M Prasad, W Yu, X Wang, Q Zhu, J. Q. Feng, R. J. Hinton, and C Qin (2010). Distribution of small integrin-binding ligand, N-linked glycoproteins (SIBLING) in the condylar cartilage of rat mandible. International journal of oral and maxillofacial surgery; 39(3), 272–281.

[24] L. R. Rodrigues, J. A. Teixeira, F. L. Schmitt, M. Paulsson, and H. Lindmark-M¨ansson (2007). The role of osteopontin in tumor progression and metastasis in breast cancer. Cancer Epidemiology Biomarkers and Prevention; 16(6), 1087-1097.

[25] G. He, S. Gajjeraman, D. Schultz, D. Cookson, C. Qin, W. T. Butler, J. Hao, and A. George (2005). Spatially and temporally controlled biomineralization is facilitated by interaction between self-assembled dentin matrix protein 1 and calcium phosphate nuclei in solution. Biochemistry; 44(49), 140–148.

[26] B. L. Foster, M Ao, C. R. Salmon, M. B. Chavez, T. N. Kolli, A. B. Tran, E. Y. Chu, K. R. Kantovitz, M Yadav, S Narisawa, J. L. Millan, F. H. Nociti Jr, and

M. J. Somerman (2018). Osteopontin regulates dentin and alveolar bone development and mineralization. Bone; 107, 196–207.

[27] G. K. Hunter and H. A. Goldberg (1993). Nucleation of hydroxyapatite by bone sialoprotein. Proceedings of the National Academy of Sciences of the United States of America; 90(18), 8562–8565.

[28] G. Baht, G. Hunter, and H. Goldberg (2008). Bone sialoprotein–collagen interaction promotes hydroxyapatite nucleation. Matrix Biology; 27(7), 600–608.

[29] J. A. R. Gordon, C. E. Tye, A. V. Sampaio, T. M. Underhill, G. K. Hunter, and H. A. Goldberg (2007). Bone sialoprotein expression enhances osteoblast differentiation and matrix mineralization in vitro. Bone; 41(3), 462–473.

[30] M. MacDougall, D. Simmons, X. Luan, J. Nydegger, J. Feng, and T. T. Gu (1997). Dentin Phosphoprotein and Dentin Sialoprotein Are Cleavage Products Ex- pressed from a Single Transcript Coded by a Gene on Human Chromosome 4. Journal of Biological Chemistry; 272(2), 835–842.

[31] W. T. Butler, M. Bhown, J. C. Brunn, R. N. D'Souza, M. C. Farach-Carson, R.-P. Happonen, R. E. Schrohenloher, J. M. Seyer, M. J. Somerman, R. A. Foster, M. Tomana, and S. Van Dijk (1992). Isolation, characterization and immunolocalization of a 53-kDal Dentin Sialoprotein (DSP). Matrix; 12(5), 343–351.

[32] A. Veis and A. Perry (1967). The phosphoprotein of the dentin matrix. Biochemistry; 6(8), 2409–2416.

[33] Y. Yamakoshi (2009). Dentinogenesis and dentin sialophosphoprotein (DSPP). Journal of Oral Biosciences; 51(3), 134–142.

[34] S. Xiao, C. Yu, X. Chou, W. Yuan, Y. Wang, L. Bu, G. Fu, M. Qian, J. Yang, Y. Shi, L. Hu, B. Han, Z. Wang, W. Huang, J. Liu, Z. Chen, G. Zhao, and X. Kong (2001). Dentinogenesis imperfecta 1 with or without progressive hearing loss is associated with distinct mutations in DSPP. Nature Genetics; 27(2), 201–204.

[35] X. Zhang, J. Zhao, C. Li, S. Gao, C. Qiu, P. Liu, G. Wu, B. Qiang, W. H. Y. Lo, and Y. Shen (2001). DSPP mutation in dentinogenesis imperfecta Shields's type II. Nature Genetics; 27(2), 151–152.

[36] J.-W. Kim and J. P. Simmer (2007). Hereditary dentin defects. Journal of Dental Research; 86(5), 392–399.

[37] P. S. Hart and T. C. Hart (2007). Disorders of human dentin. Cells Tissues Organs; 186(1), 70–77.

[38] B.L.Wang, C. Yang, X.Y. Cai, M.-J. Chen, S.Y. Zhang, B. Fang, and B. Yun (2011). Malocclusion as a common occurrence in temporomandibular joint arthroscopic disc repositioning: outcomes at 49 days after surgery. Journal of oral and maxillofacial; 69(6), 1587–1593.

[39] Dentinogenesis imperfecta. Genetic and Rare Diseases Information Center (GARD) (2017) Retrieved on 06/28/2021 from https://rarediseases.info.nih.gov/diseases/6258/dentinogenesis-imperfecta.

[40] E. D. Shields, D. Bixler, and A. M. El-Kafrawy (1973). A proposed classification for heritable human dentine defects with a description of a new entity. Archives of Oral Biology; 18(4) 543–IN7.

[41] L. S. Levin, R. J. Young, and R. E. Pyeritz (1988). Osteogenesis imperfecta type I with unusual dental abnormalities. American Journal of Medical Genetics; 31(4), 921–932.

[42] M. B. W. Neville, D. D. Damm, C. M. Allen and A. C. C. (2016). Abnormalities of Teeth. Oral and Maxillofacial Pathology; 2, 49–110.

[43] D. A. McKnight, J. P. Simmer, P. S. Hart, T. C. Hart, and L. W. Fisher (2008). Overlapping DSPP mutations cause dentin dysplasia and dentinogenesis imperfecta. Journal of Dental Research; 87(12), 1108–1111.

[44] Online Mendelian Inheritance in Man (OMIM) entry - 125490 - DENTINOGENESIS IMPERFECTA 1; DGI1. Retrieved on 06/28/2021 from https://www.omim.org/entry/125490.

[45] Online Mendelian Inheritance in Man (OMIM) entry - 125500 - DENTINOGENESIS IMPERFECTA, SHIELDS TYPE III. Retrieved on 06/28/2021 from https://omim.org/entry/125500.

[46] Dentin Dysplasia Type I - NORD (National Organization for Rare Disorders). (2021) Retrieved on 06/28/2021 from https://rarediseases.org/rare-diseases/dentin-dysplasia-type-i.

[47] Dentin Dysplasia Type II - NORD (National Organization for Rare Disorders). (2021) Retrieved on 06/28/2021 from https://rarediseases.org/rare-diseases/dentin-dysplasia-type-ii.

[48] C. Shi, N. Ma, W. Zhang, J. Ye, H. Shi, D. Xiang, C. Wu, L. Song, N. Zhang, and Q. Liu (2020). Haploinsufficiency of Dspp Gene Causes Dentin Dysplasia Type II in Mice. Frontiers in Physiology; 11, 593626.

[49] K. Andersson, B. Malmgren, E. Astrom, and G. Dahllof (2018). Dentinogenesis imperfecta type II in Swedish children and adolescents. Orphanet Journal of Rare Diseases; 13(1), 1–7.

[50] C Qin, J. C. Brunn, E Cadena, A Ridall, H Tsujigiwa, H Nagatsuka, N Nagai, and W. T. Butler (2002). The expression of dentin sialophosphoprotein gene in bone. Journal of Dental Research; 81(6), 392–394.

[51] O. Baba, C. Qin, J. C. Brunn, J. E. Jones, J. N. Wygant, B. W. McIntyre, and W. T. Butler (2004). Detection of dentin sialoprotein in rat periodontium. European Journal of Oral Sciences; 112(2), 163–170.

[52] K. Alvares, Y. S. Kanwar, and A. Veis (2006). Expression and potential role of dentin phosphophoryn (DPP) in mouse embryonic tissues involved in epithelial–mesenchymal interactions and branching morphogenesis. Developmental Dynamics; 235(11), 2980–2990.

[53] K. U. E. Ogbureke and L. W. Fisher (2006). SIBLING expression patterns in duct epithelia reflect the degree of metabolic activity. Journal of Histochemistry Cytochemistry; 55(4), 403–409.

[54] M. Prasad, Q. Zhu, Y. Sun, X. Wang, A. Kulkarni, A. Boskey, J. Q. Feng, and

C. Qin (2011). Expression of dentin sialophosphoprotein in non-mineralized tissues. The journal of histochemistry and cytochemistry; 59(11), 1009–1021.

[55] R. Zhang, F.-M. Chen, S.-L. Zhao, M.-Z. Xiao, A. J. Smith, and J. Q. Feng (2012). Expression of dentine sialophosphoprotein in mouse nasal cartilage. Archives of Oral Biology; 57(6), 607–613.

[56] K. Verdelis, Y. Ling, T. Sreenath, N. Haruyama, M. MacDougall, M. C. H. van der Meulen, L. Lukashova, L. Spevak, A. B. Kulkarni, and A. L. Boskey (2008). DSPP effects on in vivo bone mineralization. Bone; 43(6), 983–990.

[57] M. C. Embree, T. M. Kilts, M. Ono, C. A. Inkson, F. Syed-Picard, M. A. Karsdal, A. Oldberg, Y. Bi, and M. F. Young (2010). Biglycan and fibromodulin have essential roles in regulating chondrogenesis and extracellular matrix turnover in temporomandibular joint osteoarthritis. The American Journal of Pathology; 176(2), 812–826.

[58] M. J. Serrano, S. So, K. K. H. Svoboda, and R. J. Hinton (2011) Cell fate mediators Notch and Twist in mouse mandibular condylar cartilage. Archives of Oral biology; 56(6), 607–613.

[59] S. Shibata, K. Fukada, S. Suzuki, T. Ogawa, and Y. Yamashita (2002). In situ hybridization and immunohistochemistry of bone sialoprotein and secreted phosphoprotein 1 (osteopontin) in the developing mouse mandibular condylar cartilage compared with limb bud cartilage. Journal of Anatomy; 200(3), 309–320.

[60] A. Balic, D. Adams, and M. Mina (2009). Prx1 and Prx2 cooperatively regulate the morphogenesis of the medial region of the mandibular process. Developmental dynamics: an official publication of the American Association of Anatomists; 238(10), 2599–2613.

[61] A. J. Sophia Fox, A. Bedi, and S. A. Rodeo (2009). The basic science of articular cartilage: structure, composition, and function. Sports Health, 1(6), 461–468.

[62] X. Jiang, S. Iseki, R. E. Maxson, H. M. Sucov, and G. M. Morriss-Kay (2002). Tissue origins and interactions in the mammalian skull vault. Developmental Biology;241(1), 106–116.

[63] S. Ravindran and A. George (2014). Multifunctional ECM proteins in bone and teeth. Experimental Cell Research; 325(2), 148-154.

[64] L. A. Opperman (2000). Cranial sutures as intramembranous bone growth sites. Developmental Dynamics; 219(4), 472-85.

[65] T. Sreenath, T. Thyagarajan, B. Hall, G. Longenecker, R. D'Souza, S. Hong, J. T. Wright, M. MacDougall, J. Sauk, and A. B. Kulkarni (2003). Dentin sialophosphoprotein knockout mouse teeth display widened predentin zone and develop defective dentin mineralization similar to human dentinogenesis imperfecta type III. Journal of Biological Chemistry; 278(27), 24 874–24 880.

[66] Q. Zhu, M. P. Gibson, Q. Liu, Y. Liu, Y. Lu, X. Wang, J. Q. Feng, and C. Qin (2012). Proteolytic processing of dentin sialophosphoprotein (DSPP) is essential to dentinogenesis," Journal of Biological Chemistry; 287(36), 30426-30435.

[67] W. Zhang, S. Rajani, and B.-Y. Wang (2018). Comparison of periodontal evaluation by cone-beam computed tomography, and clinical and intraoral radiographic examinations. Oral radiology; 34(3), 208–218.

[68] H. Nurrohman, K. Saeki, K. M. Carneiro, Y. C. Chien, S. Djomehri, S. P. Ho, C. Qin, L. B. Gower, S. J. Marshall, G. W. Marshall, and S. Habelitz (2016). Repair of dentin defects from DSPP knockout mice by PILP mineralization. Journal of Materials Research; 31(3), 321–327.

[69] Q. Liu, N. Ma, Q. Zhu, X. Duan, H. Shi, D. Xiang, H. Kong, and H. Sun (2020). Dentin Sialophosphoprotein Deletion Leads to Femoral Head Cartilage Attenuation and Subchondral Bone Ill-mineralization. Journal of Histochemistry and Cytochemistry; 68(10), 703–718.

[70] A. Gulsahi, C. S. Paksoy, S. Ozden, N. O. Kucuk, A. R. Cebeci, and Y. Genc, (2010). Assessment of bone mineral density in the jaws and its relationship to radiomorphometric indices. Dentomaxillofacial Radiology; 39(5), 284– 289.

[71] M. Chatterjee, F. Faot, C. Correa, J. Duyck, I. Naert, and K. Vandamme (2017). A robust methodology for the quantitative assessment of the rat jawbone microstructure. International Journal of Oral Science; 9(2), 87–94.

[72] G. Mabilleau, A. Mieczkowska, H. Libouban, Y. Simon, M. Audran, and D. Chappard (2015). Comparison between quantitative X-ray imaging, dual energy X- ray absorptiometry and microCT in the assessment of bone mineral density in disuse-induced bone loss. Journal of Musculoskeletal Neuronal Interactions; 15(1), 42–52.

[73] D. Mijares, A. Kulkarni, K. Lewis, F. Yao, Q. Xi, S. Tannous, R. Dias, and R. Z. Legeros, (2012). Oral bone loss induced by mineral deficiency in a rat model: Effect of a synthetic bone mineral (SBM) preparation. Archives of Oral Biology; 57(9), 1264–1273.

[74] M. O. Tonguc, U. S. Buyukkaplan, O. Fentoglu, B. A. Gumus, S. S. Cerci, and F. Y. Kirzioglu, (2012). Comparison of bone mineral density in the jaws of patients with and without chronic periodontitis. Dentomaxillofacial Radiology; 41(6), 509–514.

[75] O. Velasco, A. W. James, G. Asatrian, M. Ajalat, T. Pritchard, S. Novshadian, A. Murthy, G. Bayani, X. Zhang, K. Ting, and C. Soo (2014). High resolution x- ray: a reliable approach for quantifying osteoporosis in a rodent model. BioResearch Open Access; 3(4), 192–196.

[76] F. Faot, M. Chatterjee, G. V. de Camargos, J. Duyck, and K. Vandamme, (2015). Micro-CT analysis of the rodent jaw bone micro-architecture: A systematic review. Bone Reports; 2, 14-24.

[77] S. Lobos, A. Cooke, G. Simonett, C. Ho, S. K. Boyd, and W. B. Edwards (2018). Assessment of bone mineral density at the distal femur and the proximal tibia by dual-energy x-ray absorptiometry in individuals with spinal cord injury: precision of protocol and relation to injury duration. Journal of Clinical Densitometry; 21(3), 338-346.

[78] B. Zhang, E. Cory, R. Bhattacharya, R. Sah, and A. R. Hargens (2013). Fifteen days of microgravity causes growth in calvaria of mice. Bone; 56(2), 290– 295.

[79] T. Tominari, R. Ichimaru, K. Taniguchi, A. Yumoto, M. Shirakawa, C. Matsumoto, K. Watanabe, M. Hirata, Y. Itoh, D. Shiba, C. Miyaura, and M. Inada (2019). Hypergravity and microgravity exhibited reversal effects on the bone and muscle mass in mice. Scientific Reports; 9(1), 1–10.

[80] K. Jiao, L. N. Niu, M. Q. Wang, J. Dai, S. B. Yu, X. D. Liu, and J. Wang (2011). Subchondral bone loss following orthodontically induced cartilage degradation in the mandibular condyles of rats. Bone; 48(2), 362-371.

[81] Y. Chen, Y. Zhang, A. Ramachandran, and A. George (2016). DSPP is essential for normal development of the dental-craniofacial complex. Journal of Dental Research; 95(3),302–310.

[82] M. Prasad Gibson, P. Jani, X. Wang, Y. Lu, and C. Qin (2014). Overexpressing the NH2-terminal fragment of dentin sialophosphoprotein (DSPP) aggravates the periodontal defects in Dspp knockout mice. Journal of Oral Biosciences; 56(4), 143–148.

[83] P. H. Jani, M. P. Gibson, C. Liu, H. Zhang, X. Wang, Y. Lu, and C. Qin (2016) Transgenic expression of Dspp partially rescued the long bone defects of Dmp1- null mice. Matrix Biology; 52-54, 95–112.

[84] M. P. Gibson, P. Jani, Y. Liu, X. Wang, Y. Lu, J. Q. Feng, and C. Qin (2013). Failure to process dentin sialophosphoprotein into fragments leads to periodontal defects in mice. European Journal of Oral Sciences; 121(6), 545-550.

[85] M. P. Gibson, Q. Liu, Q. Zhu, Y. Lu, P. Jani, X. Wang, Y. Liu, M. L. Paine, M. L. Snead, J. Q. Feng, and C. Qin (2013). Role of the NH2-terminal fragment of dentin sialophosphoprotein in dentinogenesis. European Journal of Oral Sciences; 121(2), 76-85.

[86] M. Prasad, W. T. Butler, and C. Qin (2010). Dentin sialophosphoprotein in biomineralization. Connective Tissue Research; 51(5), 404–417.

[87] World Health Organization, International collaborative research on craniofacial anomalies project, (2016). Retrieved on 03/01/2021 from https://www.who.int/genomics/anomalies/cfaproject/en/.

[88] J. Nakashima and H. Duong (2021). Radiology, Image Production and Evaluation. StatPearls [Internet].

[89] M. Pandya and T. G. Diekwisch (2019). Enamel biomimetics—fiction or future of dentistry. International Journal of Oral Science. 11(1), 1-9.

[90] H. Chen, M. M. Rogalski, and J. N. Anker (2012). Advances in functional X-ray imaging techniques and contrast agents. Physical Chemistry Chemical Physics; 14(39), 13469-13486.

[91] S. Kumar, A. Kaur, B. Karda, and R. Chibh (2019). Management of dentinogenesis imperfecta: a report of two cases. International Journal of Clinical Pediatric Dentistry; 12(5), 464–466.

[92] W. T. Butler (1998). Dentin matrix proteins. European Journal of Oral Sciences; 106(1), 204–210.

[93] W. T. Butler, J. C. Brunn, C. Qin, and M. D. McKee (2002). Extracellular

matrix proteins and the dynamics of dentin formation. Connective Tissue Research; 43(2-3), 301–307.

[94] M. Tsuchiya, Y. Sasano, M. Kagayama, and M. Watanabe (2001). Characterization of interglobular dentin and Tomes' granular layer in dog dentin using Electron Probe Microanalysis in comparison with predentin. Calcified Tissue International; 68(3), 172–178.

[95] B. Liu, Y. Wang, F. Song, M. Liu, Y. Duan, and L. Zhou (2013). Cone-beam CT evaluation of the changes in the temporomandibular joint of patients with class II division 1 subdivision malocclusion before and after twin-block treatment. West China Journal of Stomatology; 31(6), 610–614.

[96] A. D. Kolb and K. M. Bussard (2019). The bone extracellular matrix as an ideal milieu for cancer cell metastases. Cancers; 11(7), 1020.

[97] M. A. El-Brolosy and D. Y. Stainier (2017). Genetic compensation: A phenomenon in search of mechanisms. PLoS Genetics; 13(7), e1006780.

[98] S. A. Danesh-Sani, D. Tarnow, J. K. Yip, and R. Mojaver (2017). The influence of cortical bone perforation on guided bone regeneration in humans. International Journal of Oral and Maxillofacial Surgery; 46(2), 261–266